J Mater Sci (2011) 46:2821–2837
DOI 10.1007/s10853-011-5302-5

REVIEW

A wide-ranging review on Nasicon type materials

N. Anantharamulu · K. Koteswara Rao · G. Rambabu · B. Vijaya Kumar · Velchuri Radha · M. Vithal

Received: 4 November 2010 / Accepted: 17 January 2011 / Published online: 2 February 2011

Abstract Nasicons (sodium super ion conductors) are a class of solid electrolytes. Their structure, compositional diversity, evolution, and applications are reviewed. A wide range of materials is considered based on crystalline and glassy Nasicon compositions.

Introduction

Human endeavors to search for new materials with potential applications have been the signature of present day scientific and technological advancement. The needs of the society drive the scientists to expand new areas of research and the work on "energy front" is no exception. The inexpensive oil is going to last after few more years and hence the search for alternate energy sources. Since the tapping of energy from non-conventional sources such as wind, solar, or nuclear sources has certain limitation, the focus has been shifted to batteries and fuel cells for ready storage and use of energy. At present, liquid electrolytes such as $LiClO_4$ dissolved in propylene carbonate are used in lithium batteries. This electrolyte suffers from a number of major shortcomings such as limited temperature range of operation, device failure due to electrode corrosion by electrolyte solution and unsuitable shapes. A suitable solid electrolyte is required to overcome these disadvantages. Two different approaches are pursued for this purpose. In the first, a plasticizer, for example, TiO_2 or Al_2O_3 can be added to make the electrolyte from liquid to solid composite. The second approach is to synthesize solids having desired ionic conductivity and other properties [1].

In the middle of twentieth century (before 1960s), ionic conductors such as α-AgI, Ca^{2+}, or Y^{3+} substituted ZrO_2 were investigated [2]. The O^{2-} ion conductivity in Ca^{2+} or Y^{3+} stabilized zirconia was less and silver halides are not stable in air and easily decompose [2]. In 1960s, an excellent Na^+ conductor, β-alumina ($Na_2O{\cdot}11Al_2O_3$), was prepared [3, 4]. β-Alumina has a layer structure and Na^+ ions migrate between two-dimensional conductive planes only. To overcome this restriction, Hong and Goodenough et al. [5, 6] proposed a framework structure with suitable tunnel size for Na^+ migration in three dimensions of $Na_{1+x}Zr_2P_{3-x}Si_xO_{12}$ ($0 \leq x \leq 3$), named as NASICON (Sodium (Na) Super (S) Ionic (I) Conductor (CON)). These compounds ($Na_{1+x}Zr_2P_{3-x}Si_xO_{12}$) are a class of structurally isomorphous 3D framework compounds possessing high conductivity, often comparable to that of liquid electrolytes at higher temperatures. The high ionic conductivity of these materials is used in making devices such as membranes, fuel cells, and gas sensors [7–10]. In addition, their low thermal expansion behavior, host for radio active waste, fairly large surface area (hence used as catalyst supports), and ability to accommodate ions in the lattice make them worthy of investigation [11–17]. Though a few related review articles are published [1, 18], to the best of our knowledge there is no comprehensive review on this important family, viz., Nasicon. This review covers the comprehensive information related to crystalline and glassy Nasicon compositions.

N. Anantharamulu (✉)
Department of Chemistry, University at Albany, SUNY, Albany, NY 12222, USA
e-mail: anavulla@albany.edu

N. Anantharamulu · K. Koteswara Rao · G. Rambabu · B. Vijaya Kumar · V. Radha · M. Vithal
Department of Chemistry, Osmania University, Hyderabad 500007, India

Structure and compositional diversity

The special attraction of the Nasicon lies in its structure. The general formula of Nasicon composition can be written as $AMM'P_3O_{12}$ (or $AM_1M_2P_3O_{12}/AM_1M_2(PO_4)_3$) where the site "A" can be occupied by alkali ions (Li^+, Na^+, K^+, Rb^+, and Cs^+), alkaline earth ions (Mg^{2+}, Ca^{2+}, Sr^{2+}, and Ba^{2+}), H^+, H_3O^+, NH_4^+, Cu^+, Cu^{2+}, Ag^+, Pb^{2+}, Cd^{2+}, Mn^{2+}, Co^{2+}, Ni^{2+}, Zn^{2+}, Al^{3+}, Ln^{3+} (Ln = rare earth), Ge^{4+}, Zr^{4+}, Hf^{4+} and it can also be vacant. The M and M′ sites are occupied by di (Zn^{2+}, Cd^{2+}, Ni^{2+}, Mn^{2+}, Co^{2+}), tri (Fe^{3+}, Sc^{3+}, Ti^{3+}, V^{3+}, Cr^{3+}, Al^{3+}, In^{3+}, Ga^{3+}, Y^{3+}, Lu^{3+}), tetra (Ti^{4+}, Zr^{4+}, Hf^{4+}, Sn^{4+}, Si^{4+}, Ge^{4+}), and penta (V^{5+}, Nb^{5+}, Ta^{5+}, Sb^{5+}, As^{5+}) valent transition metal ions to balance the charge suitably. Phosphorous can be partially substituted by Si or As. Depending on the composition, the crystal structure can be rhombohedral (for many Nasicon systems), monoclinic, triclinic, orthorhombic, Langbeinite, Garnet, SW type (orthorhombic scandium wolframate $Sc_2(WO_4)_3$), and corundum-like. The rhombohedral structure (Fig. 1) consists of a three-dimensional rigid framework with $M(M')O_6$ octahedra and $PO_4(SiO_4)$ tetrahedra sharing common corners [5]. This 3D framework contains interconnected channels in which the mobile conducting ions are encapsulated at "A" sites. The interstitial space of the tunnels provides the conduction pathway for the mobile ion as shown in Fig. 1. The ions present in "A" position can have two different sites: type I sites (6b) situated between two $M(M')O_6$ octahedra along the *c*-axis (ribbons of $O_3MO_3AO_3M'O_3$) with a distorted octahedral coordination and type II sites (18e) located between the ribbons perpendicular to *c*-axis with a trigonal prismatic coordination. The ribbons are connected by PO_4 tetrahedra along the *a*-axis. All these compounds sharing the same topology in their framework are called Nasicons irrespective of its magnitude of conductivity or the presence of Na^+ in the compound. Structures of orthorhombic, monoclinic, triclinic, and corundum-like Nasicon polymorphs are given in Fig. 2.

Evolution of Nasicon

The crystal structure of $NaA_2^{IV}(PO_4)_3$ (A^{IV} = Ge, Ti, and Zr) was investigated by X-ray data in 1968 and it is the first report related to Nasicon family [19]. However, Hong and Goodenough et al. [5, 6] reported synthesis and characterization of $Na_{1+x}Zr_2Si_xP_{3-x}O_{12}$ ($0 \le x \le 3$) in 1976 are popularly known as Nasicon. It is a solid solution of $NaZr_2P_3O_{12}$ (abbreviated as NZP) and $Na_4Zr_2Si_3O_{12}$ (abbreviated as NZS). Its composition is derived from $NaZr_2P_3O_{12}$ by partial replacement of P by Si with Na excess to balance the negatively charged framework to yield the general formula $Na_{1+x}Zr_2P_{3-x}Si_xO_{12}$ ($0 \le x \le 3$). The crystal structure remained rhombohedral with space group $R\bar{3}c$ for all compositions except in the range $1.8 \le x \le 2.2$ where a monoclinic transition occurred with space group $C2/c$. The conductivity was found to be high

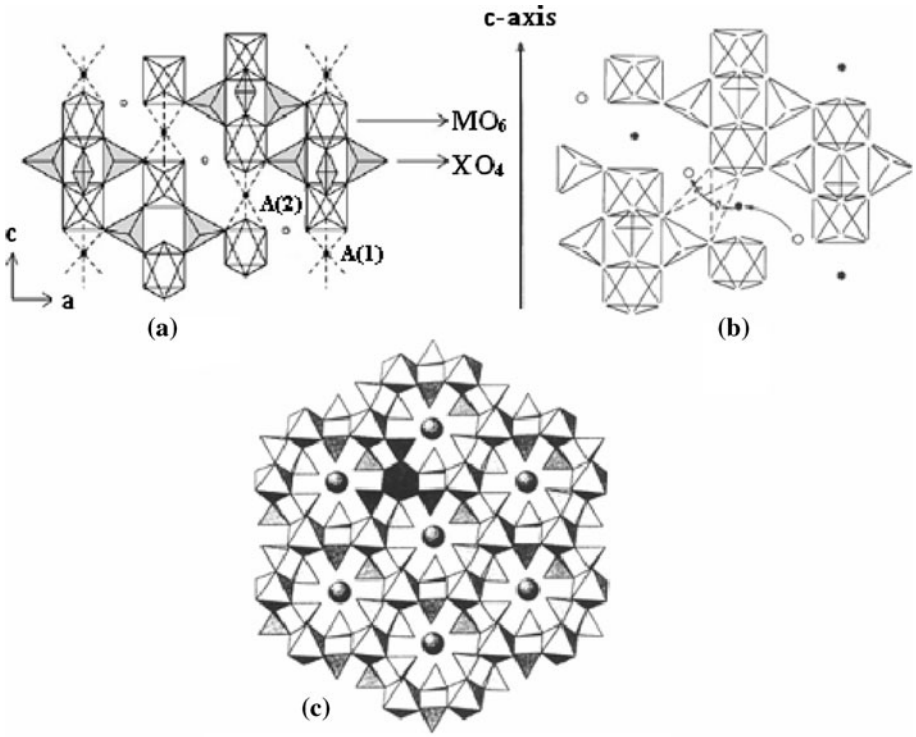

Fig. 1 The structure of Nasicon showing **a** The A1 (type 1) and A2 sites (type 2), **b** conduction pathway, and **c** hexagonal array of the $[A_2(XO_4)]$ groups in the plane (001)

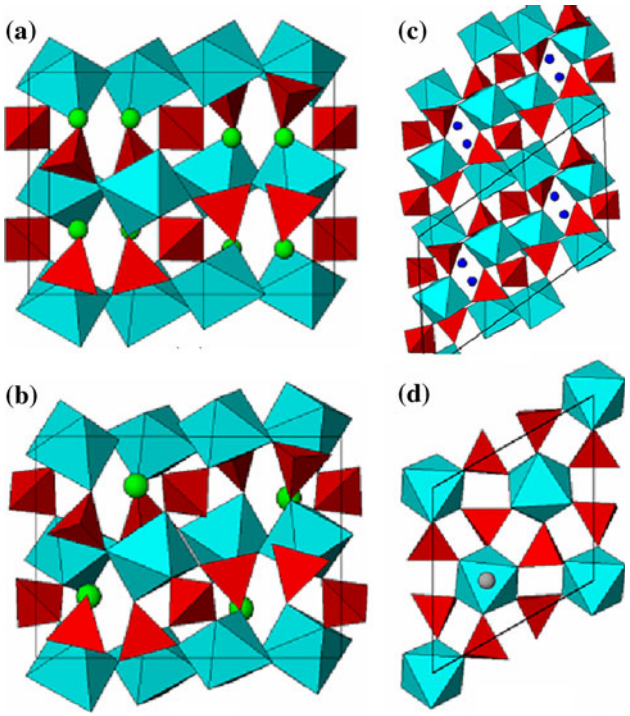

Fig. 2 Structures of Nasicon polymorphs: **a** orthorhombic (Pbna), **b** monoclinic ($P2_1/c$), **c** triclinic ($C\bar{1}$), and **d** Corundum-like

for a phase with monoclinic crystal lattice ($x = 2.0$). However, the exact composition of Nasicon prepared by high temperature solid-state reaction was contested in view of the reports of ZrO_2 impurity or other phases that appeared in the grain boundaries [20–23]. This led von Alpen et al. [24] to propose a second formula for the Nasicon solid solution namely $Na_{1+x}Zr_{2-x/3}Si_xP_{3-x}O_{12-2x/3}$. Although compositions of this type are known to exhibit an X-ray pattern of single Nasicon phase, it was also found to contain a glassy phase of low zirconium content [23]. Single crystals of rhombohedral Nasicon obtained by flux growth gave a non-stoichiometric composition $Na_{3.1}Zr_{1.78}Si_{1.24}P_{1.76}O_{12}$ upon refinement of occupation factors. In addition, the end member $x = 3$ was found to be deficient in zirconium and the charge being compensated by the presence of protons. A new general formula $Na_{1+x+4y}Zr_{2-y}Si_xP_{3-x}O_{12}$ was suggested in view of the above results [25]. Meanwhile, Clearfield et al. prepared monoclinic Nasicon by hydrothermal route and found a single phase of total composition given by X-ray fluorescence analysis as $Na_{3.3}Zr_{1.65}Si_{1.9}P_{1.1}O_{11.5}$ [26]. Similar result was obtained by powder neutron diffraction and was attributed to partial occupation of Zr^{4+} sites by Na^+ ions. All these results suggest that both stoichiometric and non-stoichiometric compounds are possible and it all depends on the method of preparation [26, 27]. Along this compositional controversy, many other Nasicons were prepared and studied. Some compositions were found to crystallize in other than rhombohedral lattice depending on the preparation method and the composition itself. Alamo has reviewed the crystal chemistry and properties of materials with NZP skeleton [28]. Properties such as ion transport, anisotropic thermal expansion, ion exchange, isomorphism, polymorphism, phase transitions, exchange and reactivities at low temperatures are presented [28]. Some discussion on the reduction of copper Nasicons is also given in this paper.

Though there is a lot of literature on Nasicons, for brevity, they can be mainly categorized based on (i) mobile ion (mono valent ions Li^+, Na^+, H^+, Cu^+, Ag^+ and di, tri and tetra valent ions) and (ii) their applications like (a) low thermal expansion materials (Ca, Sr, Ba at the site A), (b) insertion/extraction materials (presence of reducible ions like Cu^{2+}, Fe^{3+}, V^{5+}, Ti^{4+}, Nb^{5+} and a vacancy), (c) immobilization of radio active waste, (d) catalyst supports (Cu and Ag Nasicons), and (e) sensors and ion selective electrodes. For our convenience, Nasicons are classified into the following types.

Sodium containing Nasicons

After the discovery of Nasicon by Hong and Goodenough, Tran Qui et al. [29] have investigated the main diffusion pathway of Na^+ in solid solution $Na_{1+x}Zr_2P_{3-x}Si_xO_{12}$ ($x = 0$–3) between Na(1) and Na(2) from electron density maps and difference Fourier analysis. The exchange between the Na(1) and Na(2) sites remains moderate even at 620 °C. A direct relationship between the value of the conductivity and the size of the hexagonal unit cell parameter c is also established in the solid solution $Na_{1+x}Zr_2P_{3-x}Si_xO_{12}$ ($x = 0$–3) [29]. Bogusz et al. investigated the admittance spectra of $Na_{1+x}Zr_2Si_xP_{3-x}O_{12}$ for compositions $1.2 < x < 2.2$ in the frequency range from 1 Hz to 150 kHz. The spectra consist of three regions of dispersion, independent of the composition of the sample and attributed to electrode double layer, grain boundaries, and the glassy phase of Nasicon [30]. Schmid et al. have investigated the chemical stability of $Na_{1+x}Zr_2P_{3-x}Si_xO_{12}$ ($x \geq 2$) by immersion in molten sodium at 300 °C. It was confirmed that Nasicons with $x = 2$ and 2.2 were chemically attacked leading to cracking and makes the material unsuitable for use in solid electrolyte batteries in which one of the storage electrode is sodium metal [23]. Slade et al. [31] have investigated the conductivity of $Na_{1+x}Zr_2Si_xP_{3-x}O_{12}$ ($x = 2$), hydronium (H_3O^+), and ammonium Nasicons. They have noted that the conductivities of hydronium and ammonium exchanged Nasicons are dependent on pellet preparation, pretreatment, and relative humidity [31]. Bulk and grain boundary conductivities of Nasicon system, $Na_3Zr_2PSi_2O_{12}$, by complex admittance method revealed three activation energies for both the bulk and grain boundary conductivities [32].

The conductivity of $Na_3Zr_2Si_3PO_{12}$ ceramic membrane in aqueous sodium nitrate solution is measured and is found to be in accordance with the extrapolated data for Nasicon at high temperature. This proves the non-degradation of Nasicon by moisture [33]. Phase transition of $Na_3Zr_2Si_2PO_{12}$ at 450 K was investigated by longitudinal ultrasonic wave velocity and attenuation measurements [34]. A macroscopic model of temperature dependence of dielectric permittivity (ε) in the phase transition region has been proposed for $Na_3Zr_2Si_2PO_{12}$ [35].

Reports on the conductivity of single crystals of Nasicon type compounds are rare [36, 37]. The conductivity of single crystals of $NaZr_2P_3O_{12}$ is higher compared to its pellet form and found to exhibit a discontinuity at 200 °C presumably due to the transition of Na(1) to vacant Na(2) positions leading to some disorder [36]. Hydrothermal synthesis of $NaZr_2(PO_4)_3$ was carried out by Clearfield et al. from $Zr(HPO_4)_2$ H_2O [38]. Later they have prepared the same compound from $Zr(HPO_4)_2$ H_2O and Na_4SiO_4 in excess NaOH at 300 °C [39]. They concluded that the tri phosphate, $NaZr_2(PO_4)_3$, is part of a solid solution system, $Na_{1+4x}Zr_{2-x}(PO_4)_3$ with $1 > x > 0.12$ and sodium zirconium silicophosphates may also exist in zirconium deficient form.

Thin films of $NaTi_2P_3O_{12}$ and $NaZr_2P_3O_{12}$ are grown by laser ablation method. The surface morphology, composition, and crystal structure are investigated by X-ray diffraction, electron microscopy, and Rutherford backscattering spectrometry [40]. Nasicon thin film precursors are prepared by appropriate control of various processing parameters of sol–gel process [41]. Nasicon thin films are also prepared by pulsed laser deposition (PLD) and its utility as an ion selective membrane is reported [42]. Depositions of Nasicon thin films by wet as well as chemical processes with sol–gel route are also reported [41, 43–45]. Perthius et al. have prepared Nasicon thin film by screen print method [46]. A novel sol–gel processed Nasicon ($Na_3Zr_2Si_2PO_{12}$) thin film using complex precursor derived from hydroxy acid-added aqueous solutions of all inorganic materials is published [47]. Single crystal growth, structure, conductivity and its relation with structure of $Na_{1+x}Zr_2P_{3-x}Si_xO_{12}$ were reported by Boilot et al. [48]. The influence of water on the electrochemical response of a bonded Nasicon proton conductor, i.e., $Na_{1+x}Zr_2P_{3-x}Si_xO_{12}$, $x = 1.5$, Na^+ fully exchanged with H_3O^+ was studied by Gulens et al. [49]. The ac impedance studies of this proton conductor show that the conductivity is due to (1) electrode effects (2) grain boundary, and (3) grains [49, 50]. They have also demonstrated that bonded Nasicon of composition, $Na_{2.5}Zr_2P_{1.5}Si_{1.5}O_{12}$ exchanged with H_3O^+, functions effectively as a proton conductor both for hydrogen electrolysis and as a hydrogen sensor. Degradation of Nasicon at the electrode surface was observed [9].

The conductivity of silicate limits Nasicon ($Na_4Zr_2(SiO_4)_3$) in the form of thin film and its mechanical properties are reported [51]. The reaction of $Na_4Zr_2Si_3O_{12}$ (NZS) with molten sodium was reported by Gordon et al. [21]. NZS is found to be inert with molten sodium. Boilot et al. grew single crystals of $Na_5ZrP_3O_{12}$ from $Na_4P_2O_7$ flux at 1150 °C and studied its crystal structure. This zirconium deficient compound crystallizes in the Nasicon structure with space group $R\overline{3}c$ [52]. Krimi et al. reported the structure of sodium titanium phosphate, $Na_5Ti(PO_4)_3$ which crystallizes in the rhombohedral lattice with space group R32. In this titanium deficient Nasicon type compounds, one of the sodium ions occupy the site M [53].

A Nasicon-related $Na_5GdSi_4O_{12}$(NGS) and Eu^{3+} or Ce^{3+} doped (NGS) were prepared by spray freeze/freeze-drying technique to get highly dense ceramics. The bulk, grain boundary and electrode/electrolyte interface effects of NGS, Ce^{3+}/NGS and Eu^{3+}/NGS have been measured by complex plane technique. The bulk Na^+ conductivities of NGS, Ce^{3+}/NGS and Eu^{3+}/NGS were 0.21, 0.18, 0.30 S cm^{-1} at 300 °C, respectively, which are considerably higher in Nasicon family [54]. Nasicon type composition, $AM_2(PO_4)_3$ and solid solutions of $AM_{2-x}N_x(PO_4)_3$ (A = Li, Na; M, N = Ge, Sn, Ti, Zr and Hf) are prepared and studied by X-ray powder diffraction and ionic conductivity measurements [55]. The variation in conductivity with "x" is regular except in the series $NaSn_{2-x}Zr_x(PO_4)_3$, where it reaches a maximum near $x = 1$ ($\sigma = 7 \times 10^{-3}$ S cm^{-1} at 600 K) [55].

The substitution of Zr^{4+} in $Na_3Zr_2Si_2PO_{12}$ with metal ions such as Mg^{2+}, Zn^{2+}, Y^{3+} Ti^{4+}, Sn^{4+}, V^{5+}, Nb^{5+}, and Ta^{5+} and the concomitant balance of charge with excess Na^+ ions have resulted in well sintered ceramics having higher conductivities than the conductivity of Nasicon [56]. The Ti^{4+} substitution ranges for Zr^{4+} in $Na_{1+x}Zr_2P_{3-x}Si_xO_{12}$ were studied by Nakamura et al. They concluded that Ti^{4+} substitution rate was greater in phosphate-rich region than in silicate-rich region [57]. They have also investigated the characterization and electrical conductivity of $Na_{1+x}Zr_{2-y}Ti_yP_{3-x}Si_xO_{12}$ ($0 \le x \le 2$), ($y = 0$–1.5) [58].

Nasicon type composition, $Na_{3.2}Zr_2Si_{2.2}P_{0.8}O_{12}$ ($x = 2.2$), was doped with Cu^{2+}, Co^{2+}, and Zn^{2+} to obtain $Na_{3.36}Zr_{1.92}M_{0.08}Si_{2.2}P_{0.8}O_{12}$ (M = Cu, Co, and Zn). The influence of doping Cu^{2+}, Co^{2+}, and Zn^{2+} on the electrical and mechanical properties was studied. The micro hardness of the doped samples increased considerably while the variation in the bulk conductivity was found to be small [59]. Krok et al. [60] have investigated the influence of MgO and CoO doped in $Na_{3.2}Zr_2Si_{2.2}P_{0.8}O_{12}$. Both Mg^{2+} and

Co^{2+} were mainly located in the inter grain glassy phase. A series of Sc^{3+} substituted (in place of Zr^{4+}) sodium zirconium silico phosphates were prepared by Subramanian et al. Most of them crystallized in the rhombohedral lattice except $Na_3Sc_{0.5}Zr_{1.5}Si_{1.5}P_{1.5}O_{12}$, which adopted monoclinic lattice. It is suggested that when Sc^{3+} substitution for Zr^{4+} takes place, it prevents the Na^+ ions occupying the M sites [61]. Attempts to synthesize NZP compositions, $Na_{1+2x}Zr_{2-x}M_x(PO_4)_3$ ($x = 1$; M = Mg, Mn, Zn), met with mixed results. $Na_3MnZr(PO_4)_3$ and $Na_3MgZr(PO_4)_3$ were obtained in single phase while $Na_3ZnZr(PO_4)_3$ could not be prepared [62]. The conductivity and DTA studies were carried out on these two compounds. The conductivity of $Na_3MnZr(PO_4)_3$ is smaller by two orders of magnitude compared to $Na_3Zr_2Si(PO_4)_3$ while the conductivity of $Na_3MgZr(PO_4)_3$ is half of the value of Mn compound [63]. Thermal behavior of $Na_3M_2(PO_4)_3$ (M = Sc, Cr, and Fe) was examined by Rochere et al. [63]. All these compounds crystallize in three phases: (i) a high temperature rhombohedral ($R\bar{3}c$) γ-phase, (ii) an intermediate phase is either rhombohedral with superstructure for M = Sc and Fe (β-phase) or monoclinic for M = Cr (α'-phase), and (iii) a low temperature α-phase for M = Cr or Fe corresponding to an ordering of Na(1) ions. For M = Sc, powder form tend to α-Cr type. The Na^+–Na^+ correlations and phase transitions are discussed [63]. They have also investigated the synthesis, phase transitions, and ionic conductivity of $A_3M_2(PO_4)_3$ (A = Li, Na, Ag, and K; M = Cr and Fe) [64]. $Na_3Fe_2P_3O_{12}$ undergoes two reversible phase transitions: $\alpha \leftrightarrow \beta$ at 368 K and $\beta \leftrightarrow \gamma$ at 418 K related to order/disorder rearrangements on the sodium sites within the $[Fe_2P_3O_{12}]\alpha$ framework [64, 65]. The crystal structure of all the three forms has been reported [63, 66, 67]. α-form of $Na_3Fe_2P_3O_{12}$ can be synthesized by microwave method using NaH_2PO_4 $2H_2O$ [68]. $Na_3Cr_2P_3O_{12}$ undergoes three reversible phase transitions: $\alpha \leftrightarrow \alpha'$ at 348 K and $\alpha' \leftrightarrow \beta$ at 411 K and $\beta \leftrightarrow \gamma$ at 439 K related to their crystal structure [64].

Brunet et al. [69] have investigated high-pressure synthesis and in situ impedance spectroscopy of $Na_3Al_2P_3O_{12}$ in detail. This crystalline aluminum phosphate could be prepared only at high pressures. It exists in three polymorphic forms, viz., $Na_3Al_2P_3O_{12}$—I, II, III. The synthetic experiments carried out at atmospheric pressure always resulted in the formation of $AlPO_4$, Al_2O_3, and amorphous material of unknown composition [70]. This is in contrast to earlier reports on the preparation of $Na_3Al_2P_3O_{12}$ at atmospheric pressure. The phase I ($Na_3Al_2P_3O_{12}$—I) crystallizes in the pseudo tetragonal unit cell with $a = 9.313$ Å, though the splitting in the d-lines indicate symmetry based phase transitions. The phase II ($Na_3Al_2P_3O_{12}$—II, α form) prepared at pressures of 0.85–2.1 Gpa shows monoclinic deformation of the rhombohedral Nasicon cell. The third polymorph ($Na_3Al_2P_3O_{12}$—III) prepared at 1073 K, 3.9 and 6.0 Gpa crystallizes in the rhombohedral lattice and is isostructural with $Na_3Fe_2(AsO_4)_3$ (II-NaFeAs) [68]. High pressure impedance spectroscopy (HPIS) of $Na_3Al_2P_3O_{12}$—I shows low conductivity and of the order expected for amorphous (glassy) $Na_3Al_2P_3O_{12}$ and $Na_3Al_2(PO_4)_2F_3$ [70–72]. HPIS of $Na_3Al_2P_3O_{12}$—II indicates two phase transitions to true $R\bar{3}c$ Nasicon structure at 410 and 451 K, 0.4 Gpa (454 and 508 K, if pressure is 1.5 GPa) [69]. The isothermal conductivity of $Na_3Al_2P_3O_{12}$—II at 508 K is 2.5 orders of magnitude higher than the extrapolated data for $Na_3Al_2P_3O_{12}$ glass [69, 73].

Partial trivalent metal substitution at the octahedral (M) site of $AM_2P_3O_{12}$ has been widely studied. Rhombohedral $Na_{1+x}Zr_{2-x}In_xP_{3-x}O_{12}$ ($x = 0.0$–1.8) Nasicon materials have been studied by powder X-Ray diffraction (XRD), variable temperature neutron powder diffraction (NPD), ^{31}P and variable temperature ^{23}Na MAS NMR and impedance spectroscopy [74]. The compositional limit to $x = 1.8$ is due to the fact that at $x > 1.8$ more than one phase was detected [74–77]. The composition with $x = 2$, i.e., $Na_3In_2P_3O_{12}$ crystallizes in the alluaudite (solid diamond) type structure [78].

Barj et al. have reported detailed infrared and Raman spectra of Nasicon type compositions, $Na_3L_2P_3O_{12}$ (L = Fe^{3+} and Cr^{3+}) and $Na_{3+y}Cr_{2-y}Mg_yP_3O_{12}$ solid solutions [79]. The IR spectra of these compounds were characterized by ν_1, ν_2, ν_3 and ν_4 modes of phosphate group in the range 370–1200 cm^{-1} and FeO_6 (CrO_6) modes in the range 330–405 cm^{-1} [79]. The bands observed in the range 300–120 cm^{-1} were attributed to translational and vibrational modes of PO_4 group while the far IR bands observed at 85 cm^{-1} and 50 cm^{-1} are attributed to Na^+ ions in the Na(1) and Na(2) sites, respectively [79]. They observed the relation between sub lattice disorder, phase transitions, and conductivity in Nasicon compounds in the M_2O–$M_2'O$–SiO_2–P_2O_5 (M = Na, Li, K and Ag; M′ = Hf, Zr, Sc, and Ti) system in detail [80]. The Nasicon framework is described as an isolated tetrahedra sub lattice, where the M, M′ cations fill cavities between tetrahedra. The conductivity of these compounds is correlated with the structure. The lowest activation energy of conduction is observed for materials having a high degree of local disorder [80].

Losilla et al. [81] have studied the structure and electrical properties of $Na_{1.4}M_{1.6}In_{0.4}P_3O_{12}$ (M = Ti, Sn, Hf, and Zr). They have established the key structural parameters that relate the crystal structure with the Na^+ mobility and ionic conductivity. The triangle T1 formed by one O(1) and two O(2) is identified as the key bottleneck in the irregular M1–M2 conduction pathway [81].

Single crystals of zirconium deficient Nasicon type compounds in the series $Na_{1+4y+x}Zr_{2-y}P_{3-x}Si_xO_{12}$, with

the composition $Na_{5.5}Zr(Si_{0.5}P_{2.5})O_{12}$ ($x = 0.5$ and $y = 1.0$) were obtained by flux method with $Na_4P_2O_7$ as solvent. It shows two-phase transitions in the temperature range 30–200 °C [82].

Mixed valence Nasicon with Fe^{2+} and Fe^{3+} at M sites, $Na_{2+x+y}Zr_{1-y}Fe^{II}_xFe^{III}_{1-x+y}(PO_4)_3$ ($y = 0$, $0 \le x \le 1$; $x + y = 1$; $0 \le y \le 0.5$), were prepared and measured their conductivities in vacuum. Maximum conductivity of 4×10^{-3} S cm^{-1} at 300 °C was observed for $Na_{2.3}ZrFe^{II}_{0.2}Fe^{III}_{0.7}(PO_4)_3$ [83]. Asai et al. have investigated the mixed valence Nasicon compositions, $Na_{1+4x}M_xFe^{3+}_{2x}Zr_{2-3x}(PO_4)_3$ (M = Fe^{2+}, Co^{2+}, and Ni^{2+}). Their conductivity is in the order of 7×10^{-3} S cm^{-1} at 300 °C [84]. They have also examined the ionic conductivity of Nasicon type materials, $Na_{1.5}M_{0.5}Zr_{1.5}P_3O_{12}$ (M = Al, Ga, Cr, Sc, In, Fe, Yb, and Y) and concluded that the isothermal conductivity increases with increase in the ionic radius of M^{3+} ion [85]. Mixed valence Nasicons, $Na_3Zr_{0.5}M^{2+}_{0.5}Fe^{3+}P_3O_{12}$ (M = Co^{2+}, Fe^{2+}) were studied by EXAFS and XANES measurements. The population of Na^+ ions around the doped ions (Co^{2+}, Fe^{2+}, and Fe^{3+}) in these two compounds increased preferentially compared to that of Zr^{4+} [86].

Conductivity measurements of $Na_3Zr_{2-x/4}Si_{2-x}P_{1+x}O_{12}$, for $0 < x < 2$ were carried out. In these zirconium deficient Nasicon compounds, a phase transition from monoclinic to rhombohedral occurs around $x = 0.333$. It is observed that the mobility of Na^+ ions in these materials is mostly influenced by the size of the bottlenecks through which the ions have to pass. The phase transition does not affect the ionic conductivity [87].

Fast sodium ion conducting ceramic electrolyte, $Na_3Zr_{2-x}Nb_{0.8y}Si_2PO_{12}$, has been prepared by high temperature solid phase reaction. A pure single Nasicon phase with space group C2/c was found for $y < 0.5$. An unknown phase along with Nasicon was observed for $y \ge 0.5$. The results of electrical measurements indicated that the best conductivity in this system is 1.057×10^{-1} S cm^{-1} at 300 °C for the composition $y = 0.3$ and activation energy is 11.01 kJ/mole in the higher temperature range [88].

Engell et al. prepared several compositions in the Nasicon solid solution series from metal alkoxide derived gels. The effects on the polymerization and gel formation temperature, time, addition of water, and order of mixing of the components have been studied. The crystallization of gels and their usefulness as raw materials for the fabrication of dense ceramics of Nasicon have been discussed. The high temperature phase relations are also studied [89].

Porkodi et al. successfully synthesized the Nasicon compositions, $Na_{1+x}Zr_2Si_xP_{3-x}O_{12}$ ($x = 1$ and 2), by molecular precursor approach. They initially prepared the molecular precursor, $Na_{1+x}P_{3-x}Si_xO_8$ ($x = 1$ or 2) by the hydrolysis of tetraethoxysilane (TEOS) using sodium phosphate solution. Later, Nasicon precursor was obtained by reacting the molecular precursor ($Na_{1+x}P_{3-x}Si_xO_8$) with $Zr(OC_3H_7)_4$ under solvolytic condition in ethanol. Finally, the Nasicon precursor was annealed at elevated temperatures to yield phase pure Nasicon. The conductivity of as synthesized Nasicon was measured using the pellet annealed at 900 °C and found to be 5.5×10^{-3} S cm^{-1} [90].

Lithium containing Nasicons

Lithium based solid electrolytes are mainly useful for all solid state batteries due to their high energy densities and high open circuit potentials. High temperature battery applications of some of the lithium containing Nasicons have been well reviewed [1, 18]. However, this section presents more details about lithium containing Nasicons.

Among the Nasicon type series, $LiM_2(PO_4)_3$ (M = Zr, Sn, Hf and Ti), $LiZr_2(PO_4)_3$, and $LiTi_2(PO_4)_3$ are thoroughly investigated. $LiZr_2(PO_4)_3$ is known to exhibit a complex polymorphism. It is observed that $LiZr_2(PO_4)_3$ prepared above 1100 °C adopts rhombohedral structure ($R\bar{3}c$) and undergoes a phase transition to triclinic structure below 55 °C [91–93]. $LiZr_2P_3O_{12}$ may crystallize in the Nasicon or SW (orthorhombic scandium wolframate $Sc_2(WO_4)_3$) structure depending upon the synthetic temperature [94]. The enhancement of ionic conductivity at 423 K is attributed to distorted tetrahedral coordination of Li^+ coupled with the large number of empty sites available for jumping in the rhombohedral phase, which was absent in the room temperature triclinic phase [93]. Earlier results on the characterization of $LiZr_2(PO_4)_3$ gave a monoclinic unit cell parameters for this Lithium Zirconium Phosphate which is proved to be incorrect [95]. $LiSn_2(PO_4)_3$ and $LiHf_2(PO_4)_3$ also crystallize in the triclinic lattice while $LiTi_2(PO_4)_3$ crystallizes in the rhombohedral lattice. Subramanian et al. have investigated the conductivities of $LiZr_2(PO_4)_3$, $LiZr_{2-x}Ti_x(PO_4)_3$ ($x = 0.1$–2), $LiTi_2(PO_4)_3$, $Li_{1+x}Ti_{2-x}Sc_x(PO_4)_3$, and $Li_{1+x}Hf_{2-x}In_x(PO_4)_3$ [96]. It is observed that substitution of M^{3+} for M^{4+} in the series $Li_{1+x}M^{3+}M^{4+}(PO_4)_3$ (M = Zr, Ti, and Hf) increases the conductivity considerably [96].

Aono et al. have prepared $Li_{1+x}Ti_{2-x}M_x(PO_4)_3$ (M = Al, Cr, Ga, Fe, Sc, In, Lu, Y, or La) and studied their conductivity. The enhanced conductivity in M^{3+} substituted Lithium Nasicon was attributed to the densification of the sintered pellets [97]. They have also investigated the influence of addition of Li_3PO_4 or Li_3BO_3 on the conductivity of $LiTi_2(PO_4)_3$. Addition of Li_3PO_4 or Li_3BO_3 resulted in densification of sintered pellets and enhancement of the conductivity [98]. The conductivity of $Li_{1+x}Ti_{2-x}Ln_xP_3O_{12}$ (Ln = La and Lu) was also investigated by the same group [70]. They observed that the substitution of Ti^{4+} by Ln^{3+} and Li^+ decreases the porosity of $LiTi_2P_3O_{12}$ (LTPO) presumably due to the formation of

a second phase at the grain boundary which increases the density of pellets resulting an enhancement in the conductivity of Ln doped LTPO [70].

Zu-Xiang et al. have investigated the effect of M^{3+} substitution in $Li_{1+x}Ti_{2-x}M_x(PO_4)_3$ (M = In, Cr, and Ga) and $Li_{1+2x}Ti_{2-x}Mg_x(PO_4)_3$ and correlated the variation in the conductivity to polarizability (α) of M^{3+} (or Mg^{2+}) [71, 99, 100]. Later, Hamdoune et al. reinvestigated $Li_{1+x}Ti_{2-x}In_x$ $(PO_4)_3$ $(0 < x < 0.4)$ and extended to the indium rich phases $(0.4 < x < 2.0)$ [72]. Compounds with $0 < x < 0.4$, $0.4 < x < 1.0$, and $1.0 < x < 2.0$ crystallize in the rhombohedral ($R\bar{3}c$), orthorhombic (Pbca), and monoclinic ($P2_1/n$) lattices, respectively. Maximum conductivity at 300 °C was observed for $x = 0.35$ and $x = 1.8$ compositions [101]. Tran Qui et al. have demonstrated that $Li_{1+x}Ti_{2-x}Ln_xP_3O_{12}$ compounds adopt one of the above three structural types depending upon the x value [101, 102]. Wei Zhao et al. have investigated (i) conductivity of $Li_{1+x}Ti_{2-x}Al_xP_3O_{12}$ ($x = 0.3$) (LTPO:Al) and (ii) conductivity and luminescence of $Li_{1+x}Ti_{2-x}Eu_xP_3O_{12}$ (LTPO:Eu) in detail [103]. They have shown that the conductivity of LTPO:Eu is higher by 10 times to that of LTPO:Al. Luminescence and XRD studies reveal that a glassy phase of $Li_3Eu_2P_3O_{12}$ formed in the grain boundary of $LiTi_2P_3O_{12}$ decreasing the pores and increasing the contact area between the grains leading to enhancement of conductivity in LTPO:Eu compared to $LiTi_2P_3O_{12}$ [103].

Martinez et al. have studied the preparation and phase transformations of $LiSn_2P_3O_{12}$ by powder XRD, ^{119}Sn, ^{31}P, and ^{7}Li MAS NMR, conductivity (ac) and DSC techniques [104, 105]. They have noted that $LiSn_2P_3O_{12}$ exists in two phases (Phase I and II). Phase I crystallizes in monoclinic lattice ($a = 14.665$, $b = 8.405$, $c = 8.893$ Å and $\beta = 122.98°$) while phase II in rhombohedral lattice ($a = 8.642$, $c = 21.574$ Å). Calcinations of stoichiometric amounts of precursors (Li_2CO_3, SnO_2 and $(NH_4)_2HPO_4$) at 1200 °C will result in the formation of phase I while calcinations of the same precursor in the 450–1100 °C range gives phase II contaminated with SnO_2, SnP_2O_7 and Phase I. $LiSn_2P_3O_{12}$ undergoes reversible monoclinic–rhombohedral phase transformation in the temperature range 10–250 °C with a well-defined hysteresis cycle [104]. The monoclinic-to-rhombohedral phase transformation occurs in the range 120–190 °C on heating while rhombohedral to monoclinic transformation occurs between 60 and 100 °C on cooling cycle [104]. Paris et al. have investigated DSC, powder XRD, NMR (^{31}P and ^{7}Li) and ac conductivity of $LiHf_2P_3O_{12}$ [106]. These studies indicate that $LiHf_2P_3O_{12}$ exhibits a reversible first order phase transition around 0 °C. It crystallizes in the hexagonal lattice and undergoes to a triclinic distortion at 0 °C. This is perhaps the first time that a compound belonging to Nasicon family crystallizing in triclinic lattice [106]. DSC studies of $LiHf_2P_3O_{12}$ show small hysteresis, which is similar to $LiZr_2P_3O_{12}$ [107] and $LiSn_2P_3O_{12}$ [104].

The effect of addition of Li_3PO_4 or Li_2O on the conductivity of $LiM_2(PO_4)_3$ (M = Ti, Zr and Hf) was studied by Kuwano et al. and observed an increase in the conductivity [108]. The electrical properties and the crystal structure for Nasicon type solid electrolyte based on $LiHf_2(PO_4)_3$, i.e., $LiHf_2(PO_4)_3 + Li_2O$ system and $Li_{1+x}M_xHf_{2-x}(PO_4)_3$ (M = Cr, Fe, Sc, In, Lu or Y) systems have been investigated [109]. The conductivity was considerably enhanced in these systems due to the densification and decrease in the activation energy at the grain boundary [109].

Losilla et al., later investigated preparation, diffuse reflectance, and impedance spectroscopy of $Li_{1+x}M_xHf_{2-x}(PO_4)_3$ (M = Cr and Fe) [110]. It was noted that in the series $Li_{1+x}Cr_xHf_{2-x}(PO_4)_3$, rhombohedral structure exists for $x = 0.1$ and orthorhombic structure for $0.5 < x < 2.0$. In the system $Li_{1+x}Fe_xHf_{2-x}(PO_4)_3$, the orthorhombic structure exists for $0.3 < x < 1.5$. The ionic conductivity increases with the substitution of M^{3+} for Hf^{4+} ions [110].

Shi-Chun et al. have investigated the phase relationship and conductivity of $Li_{1+x}Ge_{2-x}Al_x(PO_4)_3$ and $Li_{1+x}Ge_{2-x}Cr_x(PO_4)_3$ systems [111]. It was observed single phase solid solutions of $R\bar{3}c$ structure can be formed in the range $0 \le x \le 0.6$ for Al^{3+} and $0 \le x \le 0.5$ for Cr^{3+} in $LiGe_2(PO_4)_3$. All compositions have relatively high conductivity. The electron transference numbers are around 10^{-5} for these compositions and the lithium mobility is of the order 3.5×10^{-5} cm^2 s^{-1} [111]. Nanjudaswamy et al. have investigated redox potential evaluation and electrochemical characterization of $Li_3Fe_2P_3O_{12}$, $LiTi_2P_3O_{12}$, and $Li_3FeVP_3O_{12}$ [112]. The conductivity of $LiM_2P_3O_{12}$ (M = Ge, Ti, Sn, Zr and Hf) may be increased by partial substitution of M^{4+} with trivalent cations such as Al, Ga, In, Sc, Y, La, Cr, and Fe [97, 113, 114].

Aono et al. have investigated the conductivity of $Li_{1.3}Ti_{1.7}Al_{0.3}P_3O_{12}$ and attributed its enhanced conductivity to densification of the sintered pellet and to a decrease in activation energy for the grain boundary ion transport [115, 116]. Later this system was further investigated. Substitution of (i) Al^{3+} into Ti^{4+} site, (ii) M^{+5} (V, Nb) into the P^{5+} site in the series $Li_{1+y}Al_yTi_{2-y}(PO_4)_3$ and $Li_{1+y}Al_yTi_{2-y}(PO_4)_{3-x}(MO_4)_x$ ($M = V^{5+}$, Nb^{5+}; $y = 0.1$, 0.3) gave several impurity phases such as TiO_2 (Rutile), $AlPO_4$-tridymite and TiP_2O_7 in addition to non-stoichiometric modified LTP ($LiTi_2P_3O_{12}$) [117]. The increase in the conductivity is correlated to both the incorporation of Al and the presence of vacancies in the LTP framework [117].

Low and high temperature Nasicon phases, $Li_{0.87}Hf_{2.032}P_3O_{12}$ and $LiSn_2P_3O_{12}$, are reported [118]. Neutron diffraction studies of these compounds show a phase transformation from rhombohedral ($R\bar{3}c$, $Z = 6$) at high temperature to triclinic ($P\bar{1}$, $Z = 2$) at low temperature. This result is in contrast to the earlier result of rhombohedral (high temperature) to monoclinic (low temperature) phase transition [104, 105]. Lithium and hydrogen ion transport in $A_{1-x}Zr_{2-x}Nb(PO_4)_3$ ($0 < x < 0.2$; A = Li, H) was investigated by Stenina et al. by ^1H, ^7Li, ^{31}P NMR and impedance spectroscopy [119]. Nb substitution leads to cation mobility enhancement and triclinic-rhombohedral phase transition.

Sugantha and Varadaraju have synthesized lithium Nasicons of composition, $Li_2M^{3+}M^{4+}(PO_4)_3$ (M^{3+} = Cr, Fe and In; M^{4+} = Ti, Zr and Hf), and investigated their ac conductivity. Among the systems investigated, $Li_2InTi(PO_4)_3$ shows larger conductivity and the results are discussed in terms of the polarizability of network cations [120]. Wang and Hwu have investigated crystal structure of mixed valent Titanium (III/IV) phosphate with Nasicon type structure. They have synthesized single crystals of $Li_{2.72}Ti_2P_3O_{12}$, which crystallizes in the orthorhombic unit cell. It undergoes two reversible phase transitions at 165 and 230 °C [121]. Busu et al. investigated the ionic conductivity in the system $Li_{9-4x}Zr_x(PO_4)_3$ ($0 < x < 2$) and the enhancement of conductivity with increase in the value of x [122].

Nasicon-related phases, $Li_3M_2P_3O_{12}$ (M = Cr^{3+}, Fe^{3+}, Sc^{3+} and In^{3+}), have been studied in detail [123–126]. Both $Li_3Fe_2P_3O_{12}$ and $Li_3Sc_2P_3O_{12}$ exhibit polymorphism. They exist in (i) low temperature monoclinic form, α, (ii) another monoclinic form, β, and (iii) high temperature rhombohedral form, γ [64, 123]. α-$Li_3Fe_2P_3O_{12}$ shows least ionic conductivity among the three polymorphs due to complete occupation of Li^+ ions in three sets while in the high temperature, γ-$Li_3Fe_2P_3O_{12}$ one set is fully occupied and the two other sets are only 25% full leading to enhanced conductivity [64, 123].

Nasicon type $Li_{1.4}Al_{0.4}Ti_{1.6}(PO_4)_3$ solid electrolytes were prepared by crystallization of glasses, spark plasma sintering (SPS), and conventional sintering process from nanosized precursor powders synthesized by a sol–gel route. The experimental results showed that grain size and relative density were the main factors determining the ionic conductivity of the bulk materials. The SPS technique produced ceramics with nearly 100% of the theoretical density. Maximum room temperature conductivities, 1.39×10^{-3} S cm^{-1} and 1.12×10^{-3} S cm^{-1}, of grain boundary conductivity and total conductivity, respectively, were obtained. Crystallization of ceramics from a glass was also certified as a favorable route to fabricate a bulk material with high conductivity [127]. $Li_{0.2}Nd_{0.8/3}Zr_2(PO_4)_3$ and $Li_{3-2x}Al_{2-x}Sb_x(PO_4)_3$ (x = 0.6–1.4) have been synthesized by a sol–gel process and solid state methods, respectively. The first material, $Li_{0.2}Nd_{0.8/3}Zr_2(PO_4)_3$, was characterized by TEM, neutron and powder X-ray diffraction. The Nd^{3+} ions present an ordered distribution in the $[Zr_2(PO_4)_3]$—network which leads to a doubling of the classical c parameter (a = 8.7160(3) Å, c = 46.105(1) Å). Above 600 °C, Nd^{3+} diffusion occurs at 1000 °C to the loss of the supercell [128]. The later composition, $Li_{3-2x}Al_{2-x}Sb_x(PO_4)_3$ (x = 0.6–1.4) was characterized by powder XRD and IR. DC conductivities were measured in the temperature range 300–573 K by a two-probe method. Impedance studies were carried out in the frequency region 10^2–10^6 Hz as a function of temperature (300–573 K) [129].

Copper and silver containing nasicons

Copper containing Nasicons such as $Cu^{1+}Zr_2(PO_4)_3$ and $Cu^{1+}Ti_2(PO_4)_3$ were the earliest compositions reported [130, 131]. Crystal structure of $Cu^{1+}Zr_2(PO_4)_3$ was studied by Bussereau et al. using powder XRD and neutron diffraction techniques [132]. Mbandza et al. have reported preparation, powder XRD, IR, and UV–Visible spectra of $Cu^{1+}Ti_2(PO_4)_3$ and shown that this material is isomorphous with $NaTi_2(PO_4)_3$ despite the absence of a few strong d-lines in the XRD pattern [131]. Transmission electron microscopy and catalytic activity of $Cu^{1+}Ti_2(PO_4)_3$ and $AgTi_2(PO_4)_3$ on mild oxidation of propene to acrolein were also reported [133]. Catalytic activity of $Cu^{1+}Zr_2(PO_4)_3$ in the decomposition of isopropyl alcohol was studied [134]. Later, it was demonstrated that the compound $Cu^{1+}Zr_2(PO_4)_3$ can be oxidized to form $Cu^{2+}_{0.5}Zr_2(PO_4)_3$ [135]. Detailed crystal structure, ESR, and optical spectral studies of $Cu^{2+}_{0.5}Zr_2(PO_4)_3$ were reported along with the preparation of $M_{0.5}Zr_2(PO_4)_3$ (M = Ca, Sr, Cd, and Pb) [136]. Hydrogenated copper(I) Nasicon, $H_{0.5}Cu^{1+}_{0.5}Zr_2(PO_4)_3$ was prepared by the reduction of $Cu^{2+}_{0.5}Zr_2(PO_4)_3$ in a flow of hydrogen [135]. Its crystal structure, ESR, and optical spectral studies are reported [135]. Hydrogen insertion studies of $Cu^{1+}Zr_2(PO_4)_3$ and $Cu^{2+}_{0.5}Zr_2(PO_4)_3$ by ESR and magnetic susceptibility were carried out to locate the sites occupied by Cu^+ and Cu^{2+} ions [137]. Solid state and sol–gel derived $Cu^{2+}_{0.5}Zr_2(PO_4)_3$ was studied by X and Q-band ESR and magnetic susceptibility [138]. The distribution of Cu^{2+} ions in the lattice in M_1 and M_2 sites is found to be dependent on the method of preparation [138]. EXAFS studies of $Cu^+M_2(PO_4)_3$ (M = Ti and Zr), $A_{1-x}Cu^{1+}_xZr_2(PO_4)_3$ $(0 < x \leq 1; \text{A} = \text{Na}; \quad x = 0.5, \text{A} = \text{H})$

and $Cu^{2+}_{0.5}Zr_2(PO_4)_3$ were studied by Fargin et al. [139]. In these Cu^{+} containing compounds, ($Cu^{+}Zr_2(PO_4)_3$, $H_{0.5}Cu^{1+}_{0.5}Zr_2(PO_4)_3$, $Na_{1-x}Cu^{1+}_{x}Zr_2(PO_4)_3$ $(0<x\leq 1)$) copper pairs have been detected with Cu^{I}–Cu^{I} distance of 2.40 Å. El Jazouli et al. have reported the preparation, neutron diffraction, ESR, magnetic and optical spectral studies of $Cu^{2+}_{0.5}Ti_2(PO_4)_3$ [140, 141]. Winand et al. have reported synthesis, X-ray diffraction, infrared and conductivity (ac) of Nasicon like compositions, $M^{+}N^{4+}(PO_4)_3$ (M = Ag, Cu; N = Ge, Hf, Sn, Ti, Zr) [142]. Preparation, XRD and Sn-Mossbauer of mono valent copper containing Nasicon, $Cu^{1+}Sn_2(PO_4)_3$ was reported by Serghini et al. [143]. The ionic conductivities of silver containing Nasicons are always higher than those of corresponding sodium containing Nasicons, which was explained based on polarizability of silver ion [144]. Synthesis, structure, infrared, reflectance, ESR and temperature programmed reduction of $Cu^{2+}_{0.5}Hf_2(PO_4)_3$ was reported by Ziyad et al. along with the preparation and characterization of $M^{2+}_{0.5}Hf_2(PO_4)_3 (M = Cd, Ca, Sr)$ [144].

Copper containing Nasicons, $Cu^{+}M_2(PO_4)_3$ or $Cu^{2+}_{0.5}M_2(PO_4)_3$ with tetravalent M ions occupying the Nasicon framework have been studied [135, 138]. However, copper Nasicon compositions, $Cu^{2+}_{0.5}M^{5+}N^{3+}(PO_4)_3$ or $Cu^{1+}M^{5+}N^{3+}(PO_4)_3$ were not reported in literature. We have made attempts to synthesize these new compositions and were successful in preparing $Cu_{0.5}NbAlP_3O_{12}$ (CNAP) and $Cu_{0.5}TaFeP_3O_{12}$ (CTFP). The possibility of reducing the copper and thereby facilitating the hydrogen insertion (protonation) of these Nasicons either partially or completely in place of copper, to realize proton conductors was another reason that prompted us to explore new compositions of copper Nasicons. The reduction of CNAP in the presence of hydrogen gives rise to elemental copper and $HNbAlP_3O_{12}$ (HNAP). The electron spin resonance and photoacoustic spectra of these samples are consistent with this conclusion [145]. In principle, the presence of two reducible ions in the structure should provide scope for a more hydrogen insertion. Keeping this in view, we have prepared copper and iron containing Nasicon, $Cu_{0.5}TaFeP_3O_{12}$ (CTFP), and studied the hydrogen insertion making use of ESR and Mossbauer techniques. The ESR and Mossbauer spectral results suggest only partial reduction of both Cu^{2+} and Fe^{3+} to Cu^{+} and Fe^{2+}, respectively, with simultaneous hydrogen insertion to balance the charge [146]. To verify the chances of reducing the ions that are not present in the channels, two experiments were carried out: (i) new compositions, $Ca_{0.5}NbMP_3O_{12}$ (M = Fe, Al, Ga, and In), were prepared and the iron system was investigated by Mossbauer spectroscopy. The reduction of $Ca_{0.5}NbFeP_3O_{12}$ in hydrogen atmosphere gave $Ca_{0.5}HNbFe_{1-x}(III)Fe_x(II)P_3O_{12}$, which on heating in air gives back $Ca_{0.5}NbFeP_3O_{12}$ [147]. (ii) A known composition, $CaTiFeP_3O_{12}$, was prepared and the reduction of Fe^{3+} present in the framework was studied by Mossbauer spectroscopy. It was observed that $CaTiFeP_3O_{12}$ could not be reduced completely due to double the number of Ca^{2+} present in this material compared to $Ca_{0.5}NbFeP_3O_{12}$ [148].

Compared to sodium (or lithium) containing Nasicons, silver containing Nasicons are less studied. After the preparation of silver exchanged original Nasicon by Hong et al., it was Perret and Boudja who have for the first time reported silver containing Nasicon, $AgSn_2P_3O_{12}$ [149]. Later silver Nasicons, $AgZr_2P_3O_{12}$ and $AgTi_2P_3O_{12}$, were prepared [133, 150–153]. Preparation and selective catalytic oxidation of hydrocarbons using $M^{+}Ti_2P_3O_{12}$ (M = Ag and Cu) as catalysts are reported by Oudet et al. [133]. Arsalane et al. have studied catalytic activity of $AgZr_2P_3O_{12}$ in the butan-2-ol conversion to butanes and methyl ethyl ketones [154]. For the same reaction, Youness Birk et al. have reported the catalytic behavior of $AgHf_2P_3O_{12}$ [13]. They have concluded that the dehydration activity of $AgHf_2P_3O_{12}$ was higher than that of $AgZr_2P_3O_{12}$ presumably because Hf enhances the acid properties of phosphate more strongly than Zr [13]. d'Yvoire et al. have reported the preparation and conductivity of $Ag_3M_2P_3O_{12}$ (M = Cr and Fe). $Ag_3Fe_2P_3O_{12}$, prepared by ionic exchange method undergoes a reversible phase transition $\beta \leftrightarrow \gamma$ at 346 K while $Ag_3Cr_2P_3O_{12}$ does not undergo any such transition [63, 64].

We have investigated the preparation, characterization, and electrical properties of new silver Nasicons, $AgTaMP_3O_{12}$ (M = Al, Ga, In, Cr, Fe and Y), $AgSbMP_3O_{12}$ (M = Al, Ga, Fe and Cr), and $Ag_{3-2x}Ta_xAl_{2-x}(PO_4)_3$ (x = 0.6 to 1.4). The Cole–Cole plots do not show any spikes on the lower frequency side indicating negligible electrode effects. The isothermal conductivity obtained from dc (σ_{dc}) and ac ($\sigma(0)$) agrees well. The activation energies obtained from the plots of log $\sigma_{dc}T$ vs. $1/T$, log $\sigma(0)$ vs. $1/T$, and log τ vs. $1/T$ are approximately same suggesting conducting species to be mobile silver ions. The room temperature Mossbauer spectrum of $AgTaFeP_3O_{12}$ suggests paramagnetic nature of this sample [155–157].

Mixed and multi valent Nasicons

A non-stoichiometric Nasicon, $Na_{0.5}Nb_2P_3O_{12}$, containing mixed valence of niobium [(Nb(V) and Nb(IV)] has been synthesized and its crystal structure investigated [158]. This non-stoichiometric compound was found to be isostructural with stoichiometric mixed valence $Nb_2P_3O_{12}$ [159]. Nasicon compounds with mixed valence of titanium ($Na_{1+x}Ti_2P_3O_{12}$) were synthesized by (i) solid state,

(ii) electrochemical, and (iii) reaction with organo-metallic compounds [160, 161]. Mixed valent vanadium containing Nasicons were prepared by Gopalakrishnan and Kasturi Rangan. It was achieved by oxidation of $Na_3V_2P_3O_{12}$ by bubbling chlorine gas in $CHCl_3$. Sodium was de-intercalated from $Na_3V_2P_3O_{12}$ lattice to get $V(IV)V(V)P_3O_{12}$ in good yield. They also successfully prepared $NaV_2P_3O_{12}$, $Li_{0.86}V_2P_3O_{12}$, $Li_{2.4}V_2P_3O_{12}$, $Li_3V_2P_3O_{12}$, and $H_3V_2P_3O_{12}$ using this deintercalation technique [17]. All these compounds were found to crystallize in rhombohedral lattice and isomorphous with $Na_3V_2P_3O_{12}$.

Nasicon type compositions, $NaABP_3O_{12}$ (A^{5+} = Nb, Ta; B^{3+} = Ti, V, Cr, Fe, Al), $LiNbMP_3O_{12}$ (M^{3+} = V, Fe) and $LiTaMP_3O_{12}$ (M^{3+} = V, Cr, Fe, Al), were prepared and characterized by Gopalakrishnan. All these materials crystallize in rhombohedral lattice except $LiNbVP_3O_{12}$ and $LiTaVP_3O_{12}$, which crystallize in monoclinic lattice [162, 163]. Berry et al. have presented the synthesis and characterization of $NaM'M''P_3O_{12}$ (M' = Nb, Sb; M'' = Al, Ga, In, and Fe). All these materials also crystallize in rhombohedral lattice [164]. Compounds of general formula $A^+M_2^{3+}(Me^{5+}O_4)_3$ (A = Li, Na, Ag or K; M^{3+} = Ga, Cr, Fe, Al, Sc, or In and Me^{5+} = P or As) have been studied. Sodium phosphates of composition, $Na_3M_2P_3O_{12}$ (M^{3+} = Fe, Cr, V, Sc), crystallize in the hexagonal lattice with space group $R\bar{3}c$. All these phosphates exhibit monoclinic modification at low temperatures [160, 165].

Sugantha et al. have synthesized a series of isostructural compounds belonging to NZP family by solid-state route [166]. The compositions prepared are $ATiMP_3O_{12}$, $AZrMP_3O_{12}$ (A = Ca, Sr, Ba, and M = Fe, In, and Cr), $Nb(V)Nb(IV)P_3O_{12}$ and $ATi(IV)Ti(III)P_3O_{12}$ (A = Ca, Sr, Ba). All these compositions crystallize in rhombohedral lattice. (i) Detailed IR studies of all the compositions, (ii) UV–Visible and Diffuse reflectance spectra (DRS) of $ABFeP_3O_{12}$ (A = Ca, Ba, Sr; B = Ti, Zr), (iii) DC magnetic susceptibility of $BaTiMP_3O_{12}$ ($M = Ti^{3+}$, Fe^{3+}), $SrTiFeP_3O_{12}$, $SrZrFeP_3O_{12}$, $BaZrFeP_3O_{12}$, and (iv) ESR of $ATi^{4+}Ti^{3+}P_3O_{12}$ (A = Ca, Sr, Ba) and $NbNbP_3O_{12}$ are reported [166]. Multivalent cationic conduction in crystalline Nasicon phases was studied [167]. In these Nasicons, trivalent cations like Al^{3+}, Sc^{3+}, Ce^{3+} and rare earth ions and tetravalent ions like Zr^{4+} and Hf^{4+} were found to be the conducting species by EPMA studies [168–172]. An extraordinary high Al^{3+} ion conductivity was realized in the Nasicon type structure $(Al_xZr_{1-x})_{4/(4-x)}Nb(PO_3)_4$ by Imanaka et al. [173]. The Al^{3+} ion conductivity in this material is considerable higher than the conductivity observed in $Sc_{1/3}Zr_2(PO_4)_3$ and comparable to yttria-stabilized zirconia (YSZ) and calcia-stabilized zirconia (CSZ). Trivalent rare earth ion conducting phosphates, $(R_xZr_{1-x})_{4/(4-x)}NbP_3O_{12}$ (R = La, Nd, Gd) and $(R_{0.1}Zr_{0.9})_{(40+10x)/39}NbP_{3-x}Si_xO_{12}$ (R: Rare earth) were studied by the same group [173, 174]. Among the series, $(Nd_xZr_{1-x})_{4/(4-x)}NbP_3O_{12}$ shows highest conductivity of 10^{-4} S cm^{-1} at 600 °C. The conducting species is found to be Nd^{3+} by ac conductivity measurements in various oxygen partial pressures and also by dc electrolysis [173]. They have also studied the pure tetravalent M^{4+} (M = Ti, Zr, and Ge) ion conduction in $Ti(Nb_{1-x}W_x)_{5/(5+x)}(PO_4)_3$, $Zr_{1+x/4}TaP_{3-x}Si_xO_{12}$ and $GeNb(PO_4)_3$ for the first time [174–177]. In Ti-Nasicon, W^{6+} was partially substituted onto the Nb^{5+} site to obtain high Ti^{4+} ion conductivity by reduction of the strong electrostatic interaction between the Ti^{4+} cation and the surrounding counter O^{2-} anions [175]. Zr^{4+}-ion conducting Nasicon was developed by partially substituting the P^{5+} ions in the Nasicon-type $ZrTa(PO_4)_3$ solid with Si^{4+} ions having larger ionic size and lower valence [176]. Tetravalent Ge^{4+} ion conduction was demonstrated by partial replacement of P^{5+} ion in $GeNb(PO_4)_3$ by Si^{4+} ion [177]. Similarly, they have also developed the tetravalent hafnium ion conducting Nasicons, $HfNbP_{3-x}V_xO_{12}$ and $Hf_{1-y/4}NbP_{3-y}W_yO_{12}$ by partial replacement of P^{5+} ions by larger V^{5+} or W^{6+} ions, resulted in an enhancement in conductivity due to the expansion of Hf^{4+} ion conducting pathways in $HfNb(PO_4)_3$ [178]. Orlova et al. have investigated the Nasicon (NZP) type microcrystals, $Th_{1/4}Zr_2(PO_4)_3$ by Pechini type sol–gel method at 900 °C. They stated that actinide phosphates lead to potential applications in the field of radionuclide immobilization [179].

Chromium (Cr^{3+}) substituted Nasicons, $Na_{1+x}Cr_xM_{2-x}(PO_4)_3$ (M = Ti, Hf, and Zr) and $A_{(1+x)/2}Cr_xM(PO_4)_3$ (A = Cd, Ca, and Sr) have been characterized by powder X-ray diffraction, ^{31}P-MAS NMR, and infrared spectroscopy [180]. The strength of the P–O bonds are affected by A and M ions in these phosphates [180]. Chakir et al. have synthesized $Na_3MZrP_3O_{12}$ (M = Mg, Ni) by co precipitation method at 750 °C and characterized by Raman and powder XRD [181]. Ion exchange of this sodium Nasicon gave $Li_{2.6}Na_{0.4}NiZrP_3O_{12}$ which was also characterized. Diffused reflectance spectra indicate the presence of Ni^{2+} in octahedral coordination [181]. Synthesis and crystal structure of Co^{2+} doped $Na_{3+x}Cr_{2-x}Co_xP_3O_{12}$ ($0 \le x \le 1$) was studied by the same group [182]. The composition, $Na_{3.5}Cr_{1.5}Co_{0.5}P_3O_{12}$ crystallizes in rhombohedral lattice with $R\bar{3}c$ space group. The infrared spectra of lithium iron phosphates including $Li_3Fe_2(PO_4)_3$ was reported by Salah et al. [183]. The internal and external modes of vibrations are analyzed to distinguish different phases and the type of cationic environment in the framework [183]. Mariappan et al. have investigated the synthesis of nano structured $LiTi_2(PO_4)_3$ by pechini-type polymerizable complex

method using soluble ammonium citratoperoxotitanate. The particle size measured from XRD patterns and transmission electron microscopy (TEM) was in the range 50–125 nm [184].

Nasicon compositions, $AFeSnP_3O_{12}$ (A = Na_2, Ca, Cd) and $AFeTiP_3O_{12}$ (A = Ca and Cd), were prepared by solid state method and their structures were determined by XRD using Rietveld analysis [185]. All these compounds crystallize in rhombohedral lattice ($R\bar{3}c$ space group) with random distribution of Sn(Fe) (or Sn(Ti)) within the framework. It is observed that partial occupancy of M1(Na(1)) and M2(Na(2)) sites in $Na_2FeSnP_3O_{12}$ leading to cationic distribution $[Na_{1.22-1.78}]_{M2}[Na_{0.78-0.22}]_{M1}]SnFeP_3O_{12}$, Ca (in $CaFeSnP_3O_{12}$ and $CaFeTiP_3O_{12}$) and Cd (in $CdFeSnP_3O_{12}$ and $CdFeTiP_3O_{12}$) are found to occupy M1 sites [185, 186]. The preparation, structure determination, and thermal expansion of $Ca_{1-x}Sr_xZr_4P_6O_{24}$ ($0 \leq x \leq 1$) were carried out by Fischer et al. No structural transformation has been observed by high temperature XRD up to 1000 °C [187].

Aatiq et al. have reported the crystal structures of ortho phosphates, $Ca_{0.5}SbFe(PO_4)_3$ and $CaSb_{0.5}Fe_{1.5}(PO_4)_3$, obtained by conventional solid state reaction method at 900 °C. Both these compounds belong to the Nasicon family and crystallized in hexagonal lattice with the space group $R\bar{3}$ and $R\bar{3}c$, respectively [188]. They have also studied the synthesis and crystal structures of $A_{0.5}SbFe(PO_4)_3$ (A = Mn, Cd), obtained by solid state reaction at 920 °C and their crystal structure possesses hexagonal lattice with the space group $R\bar{3}c$ [189].

Arbi et al. have prepared the titanium-based Nasicons, $Li_{1+x}Ti_{2-x}Al_x(PO_4)_3$ and $LiTi_{2-x}Zr_x(PO_4)_3$ and studied with X-ray Diffraction (XRD), Nuclear Magnetic Resonance (NMR) and Electric Impedance (EI) techniques. From the analysis of the ^7Li and ^{31}P NMR spectra, cation distribution and Li mobility have been deduced [190]. Essoumhi et al. have reported the synthesis and characterizations of Nasicon type ionic conducting ceramics, $Na_{1+x}M_{1.775}Si_{x-0.9}P_{3.9-x}O_{12}$ with $1.8 \leq x \leq 2.2$ and M = Zr or Hf. The effect of the total substitution of zirconium by hafnium on electric properties has been studied. The various compositions were prepared by using the sol–gel method and the synthesized precursors were characterized by coupled DTA–TG [191]. Benmokhtar et al. have synthesized the new Nasicon type iron titanyl phosphate $Fe_{0.50}Ti_2(PO_4)_3$ by both solid-state reaction and Cu^{2+}–Fe^{2+} ion exchange method [192]. The material was then characterized by X-ray diffraction, Mössbauer, magnetic susceptibility measurements and optical absorption. The crystal structure of the compound was refined, using X-ray powder diffraction data, by the Rietveld profile method; it crystallizes in the rhombohedral system, space group $R\bar{3}$, with $a = 8.511(1)$ Å and $c = 20.985(3)$ Å, $V = 1316.45(3)$ Å^3 and $Z = 6$. It's structure is comparable to that of $Mn_{0.50}Ti_2(PO_4)_3$. Mössbauer studies showed that the presence of one Fe^{2+} site in the high spin state ($t_{2g}^4e_g^2$). The Curie–Weiss-type behavior is observed in the magnetic susceptibility. Diffuse reflectance spectrum indicates the presence of octahedrally coordinated Fe^{2+} ions [192]. Barré et al. have investigated the synthesis and structure of a new Nasicon type solid solution, $Li_{1-x}La_{x/3}Zr_2(PO_4)_3$ ($0 \leq x \leq 1$). These phases were synthesized by a complex polymerizable method and structurally characterized from Rietveld treatment of their X-ray and neutron powder diffraction data. This solid solution results from the substitution mechanism $Li^+ \rightarrow 1/3La^{3+} + 2/3$ leading to an increase of the vacancies number correlated to an increase of the La content [193].

Blue luminescent material, $Eu_{0.5}Zr_2(PO_4)_3$, belongs to Nasicon family was prepared by solid state method [194]. This is the first instance of Eu^{2+} occupying the "A" site in the Nasicon framework structures. The emission studies of this material are carried out. We have studied conductivity and luminescence of Eu^{3+} doped Nasicon compositions, $Ca_{0.5}Fe_{1-x}Eu_xSb(PO_4)_3$ ($x = 0.1$, 0.15, and 0.2) [195]. These compositions are prepared by Pechini type semi-sol–gel method and characterized by powder X-ray diffraction. An enhancement in conductivity is observed by doping the larger ions like Eu^{3+} in place of smaller M^{3+} (Fe^{3+}) ions. The luminescence properties and local structure of Eu^{3+} ions are derived by means of emission spectra and phonon sidebands. The electron–phonon coupling strength values are found to be more in crystalline Nasicon systems in comparison to the glassy Nasicon systems [195].

Glasses with Nasicon composition

The general formula of Nasicon ($A_xB_yP_3O_{12}$) can be written as $A_2O{\cdot}BO_2{\cdot}1.5P_2O_5$. In this composition, P_2O_5 is a glass former and alkali oxides are glass modifiers. Under suitable conditions and depending on the nature of oxide of B, this composition can give rise to glassy materials. Compared to their crystalline counterparts, studies on the Nasicon glasses are meager. Susman et al. obtained Nasicon in the vitreous form for the first time with a reduced ZrO_2 composition in $Na_{1+x}Zr_{2-x/3}Si_xP_{3-x}O_{12-2x/3}$ ($x = 3$) i.e., $2Na_2O{\cdot}ZrO_2{\cdot}3SiO_2$, with high conductivity ($\sim 2 \times 10^{-3}$ S cm^{-1} at 300 °C) and activation energy of 0.55–0.61 eV. This glass, called Nasiglas, is resistant to immersion in molten sodium and sodium poly sulfide at 300 °C [196]. Sobha and Rao prepared a series of glasses with Nasicon compositions such as $A_3Fe_2P_3O_{12}$ (A = Li, Na, and K), $A_3Ga_2P_3O_{12}$ (A = Na and K), $A_5TiP_3O_{12}$ (A = Li and Na), $A_5GeP_3O_{12}$ (A = Li and Na),

$A_4NbP_3O_{12}$ (A = Na and K) and $Na_4VP_3O_{12}$ and investigated their ac conductivities [197, 198]. The total conductivity of these glasses follow double power law ($s_1 = 0.5$ and $s_2 = 1.0$) and is independent of nature and concentration of cations and structure of the glass. They have also investigated the IR and fluorescence spectra of glassy $LiSn_2P_3O_{12}$, $NaSn_2P_3O_{12}$, and $KSn_2P_3O_{12}$ and crystalline $NaSn_2P_3O_{12}$ phases [199]. They have also investigated the fluorescence studies of Dy^{3+} and Tb^{3+} doped $Na_5TiP_3O_{12}$ and $Na_4NbP_3O_{12}$ glasses. The energy transfer between Dy^{3+} and Tb^{3+} in these glasses, nature of energy transfer and concentration limits of quenching was presented [200].

Our group members have investigated the emission spectra of Pr^{3+}, Eu^{3+}, and Dy^{3+} doped $Na_3TiZnP_3O_{12}$ glass system [201]. Rare earth ions occupy 8-9 coordination in this glass matrix. The excitation spectra of Eu^{3+}/$Na_3TiZnP_3O_{12}$ glass gave a phonon-assisted side band with phonon energy of 1022 cm^{-1}, which agrees with the IR data [201]. The optical, thermal, and conductivity studies of Nasicon type $Na_2PbZnMP_3O_{12}$ (M = Al, Ga and Fe) were also carried out by our group [202]. Physical properties such as refractive index, optical band gaps, Urbach energies, oxide ion polarizability, dc electrical conductivity, and DSC of these glasses are reported [202]. The optical spectral studies of Pr^{3+}, Nd^{3+}, Sm^{3+}, Dy^{3+}, Ho^{3+}, and Er^{3+} doped in $Na_4AlZnP_3O_{12}$ glass were reported from our laboratory [201]. Prakash et al. have investigated the physical and optical properties of Nasicon type glasses, $Na_4AlZnP_3O_{12}$, $K_4AlZnP_3O_{12}$, $Na_4AlCdP_3O_{12}$, $Na_4AlCaP_3O_{12}$, $Na_3TiZnP_3O_{12}$, $K_3TiZnP_3O_{12}$, and $Na_3TiCdP_3O_{12}$ [203]. Parameters such as refractive index, reflection loss, molar reflectivity, oxide ion polarizability, dielectric constant, optical band gap, and Urbach energies of these glasses were evaluated. A novel technique, frequency domain interferometry, has been employed to determine refractive indices over the transparency region for these glasses [204]. Govindraj and Mariappan have studied ac conductivity of Nasicon type glassy compositions, $Na_3TiZnP_3O_{12}$, $Na_3TiCdP_3O_{12}$, $Na_4AlCdP_3O_{12}$, $Na_4FeCdP_3O_{12}$, $Na_3Al_2P_3O_{12}$, $Na_5TiP_3O_{12}$, $Na_5Cu_2P_3O_{12}$, $Na_6FeP_3O_{12}$, and $Na_6AlP_3O_{12}$ [73, 205]. The ac conductivity of these glasses shows power law feature and scaling behavior [73, 205]. Mariappan et al. have also studied conductivity behavior of glassy compositions, $A_3TiB'P_3O_{12}$ (A = Li, K; B′ = Zn, Cd) and $K_3M_2P_3O_{12}$ (M = B, Al, and Bi) [206, 207].

Xu et al. have synthesized the lithium–ion conducting $Li_{1.4}Al_{0.4}Ti_{1.6}(PO_4)_3$ glass–ceramics with ultrapure Nasicon type phase by a citric acid-assisted sol–gel method and characterized with TGA-DSC, XRD, transmission electron microscopy (TEM), field emission scanning electron microscopy (FESEM) and complex impedance techniques [208]. The influence of molar ratio of citric acid to cations as well as pH value on the formation of $Li_{1.4}Al_{0.4}Ti_{1.6}(PO_4)_3$ sol was studied. Experimental results indicated that the citric acid-assisted sol–gel method made it possible to obtain well crystallized glass–ceramics of $Li_{1.4}Al_{0.4}Ti_{1.6}(PO_4)_3$ at a much lower temperature within a shorter synthesis time in comparison to conventional solid-state reaction methods [208].

Nagamine et al. prepared the glasses with composition, $37.5Li_2O$–$(25 - x)Fe_2O_{3-x}Nb_2O_{5-37.5}P_2O_5$ (mol%) (x = 5, 10, 15) and developed the Nasicon-type $Li_3Fe_2(PO_4)_3$ crystals through the conventional crystallization in an electric furnace. They found that the addition of Nb_2O_5 led to glass formation effectively. They stated that crystallization of glass precursor is a new route for the fabrication of $Li_3Fe_2(PO_4)_3$ crystals, which can be used as electrolyte in lithium ion batteries [209].

Zhang et al. studied the new sodium-ion conducting glass–ceramics composed of $Na_{1+x}Al_xGe_{2-x}P_3O_{12}$ ($0.3 \leq x \leq 1.0$) crystalline conducting phase with Nasicon type structure. They have characterized the materials with DSC, XRD, SEM, FTIR, and electrochemical impedance spectroscopy techniques. The reasons for the enhancement of the conductivity in glass–ceramics were discussed in view of the microstructure morphology and heating conditions [210].

Okura et al. investigated the glass–ceramics of titanium-, germanium- or tellurium-containing $Na_5RSi_4O_{12}$-type (R = rare earth; Y) Na^+-superionic conductors (N5YXS) by crystallization of glasses with the composition, $Na_{3+3x}Y_{1-x}X_ySi_{3-y}O_9$ (X = Ti; NYTiS, Ge; NYGeS, X = Te; NYTeS). They studied the effects of X elements on the separation of the phase and the microstructural effects on the conduction properties of glass–ceramics. They explained the enhancement of electrical conductivity in glass–ceramics, i.e., grain growth leads to high conductivity in glass–ceramics [211].

Applications of Nasicons

Metal insertion

Metal insertion studies on $NaZr_2P_3O_{12}$ (NZP) type materials possessing vacant tunnel (absence of any ion in Na site of Nasicon) are reported [212–215]. Subba rao et al. have investigated characterization, IR and isothermal resistivity of $A_xNbTiP_3O_{12}$ [A = Li, Mg, Sn, Pb, Zn, Y, Fe, Ti, Nb]. They have shown that most of the electropositive elements of periodic table can be inserted into $NbTiP_3O_{12}$ framework. The guest ion occupies the channels present in the framework structure of $NbTiP_3O_{12}$. Berry et al. have reported detailed structural and

Mossbauer studies of Fe and Sn inserted $NbTiP_3O_{12}$. Both Fe and Sn are accommodated as Fe^{2+} and Sn^{2+} in two types of sites in the channels of $NbTiP_3O_{12}$ lattice.

Electrode materials

Electrochemical or alkali metal intercalation of $ATi_2(PO_4)_3$ (A = Na, Li) has been carried out by Delmas et al. to yield $A_3Ti_2(PO_4)_3$ (A = Na, Li). The distribution of Li in $Li_3Ti_2(PO_4)_3$ is peculiar. In this compound, M_1 site is empty and M_2 is completely occupied, in contrast to $ATi_2(PO_4)_3$ (A = Na, Li) where the M_1 is fully occupied by A ions and M_2 is vacant [16].

Orthorhombic $Li_3Ti_2(PO_4)_3$ and $Li_3(V_{1-x}Zr_x)_2(PO_4)_3$ have been used as cathode materials. The discharge capacity of Zr substituted $Li_3(V_{1-x}Zr_x)_2(PO_4)_3$ samples became much larger than that of pure $Li_3Ti_2(PO_4)_3$ [216]. Electrochemical behavior of monoclinic $Li_3V_2(PO_4)_3$ and $Li_xV_2(PO_4)_3$ have been investigated by Saidi et al. [217, 218]. A combined computational and experimental study of structure and electrochemical properties of monoclinic and rhombohedral $Li_xM_2(PO_4)_3$ (with a focus on M = V) have been reported by Morgan et al. [219, 220]. Charge ordering in monoclinic $Li_3V_2(PO_4)_3$ has been investigated by Yin et al. by using it as cathode material in lithium ion batteries [221, 222].

Aatiq et al. have studied electrochemical lithium intercalation, ^{31}P NMR and powder XRD of $Mn_{(0.5-x)}Ca_xTi_2(PO_4)_3$ ($0 \leq x \leq 0.5$). The electrochemical lithium intercalation of $[A_{0.5-0.5}]_{M1}Ti_2(PO_4)_3$ shows that intercalation occurs preferentially into the empty M_1 site around 2.9 V and then into the M_2 site in the voltage range of 2.5–2.3 V [223]. They have also reported structural and electrochemical behavior of $Li_{0.5}Mn_{0.5}Ti_{1.5}Cr_{0.5}(PO_4)_3$. It was observed that Li and Mn occupy statistically the M_1 sites and the lithium ions electrochemically intercalated in this structure are localized in M_2 site [224].

Low thermal expansion

Nasicon type materials show low thermal expansion behavior, which was exploited in some of the applications of these materials. These materials are considered as attractive candidates for thermal shock, high-energy lasers, precision optics household ovenware and giant telescope mirrors [225, 226]. The reports pertaining to the thermal expansion studies are summarized below. Alamo and Roy have reported the thermal expansion behavior of compositions $Na_{1+x}Zr_2P_{3-x}Si_xO_{12}$ ($0 \leq x \leq 1$) and $Na_{1+4z}Zr_{2-z}P_3O_{12}$ ($0 \leq Z \leq 0.5$). The thermal expansion is found to be dependent on the composition and the lowest value of thermal expansion coefficient, α, was found for $x = 0.33$ and $z = 0.125$ compositions [225]. Roy et al. have reported near zero thermal expansion ceramic materials belonging to CTP family (the compositions belonging to $CaTi_4P_3O_{12}$ structure are abbreviated as CTP). Table 1 gives the thermal expansion coefficients of some of the Nasicon materials [226, 227]. Agrawal and Stubican have reported the preparation of single phase $Ca_{0.5}Zr_2P_3O_{12}$, its thermal expansion behavior and the effect of MgO and ZnO addition on the sintering behavior and thermal expansion characteristics [228]. Thermal expansion study of $AZr_2P_3O_{12}$ (A = Li, Na, K, Rb and Cs) by high temperature X-ray diffractometry and dilatometry were reported by Lenain et al. [229]. Some of the members of this NZP family exhibited very low thermal expansion coefficients ($<1 \times 10^{-6}$) including some negative values. The composition $LiZr_2P_3O_{12}$ shows a phase transition around 60 °C [230]. Limaye et al. have studied the preparation and thermal expansion of $M_{0.5}Zr_2P_3O_{12}$ (M = Mg, Ca, Sr, and Ba) [230]. These materials were synthesized by solid state and sol–gel methods. Thermal expansion study was carried out by dilatometry, high temperature X-ray diffractometry, and laser speckle techniques. The compositions $Ca_{0.5}Zr_2P_3O_{12}$ and $Sr_{0.5}Zr_2P_3O_{12}$ have exhibited negative and positive thermal expansion coefficients, respectively [230]. Srikanth et al. have investigated thermal expansion anisotropy and acoustic emission studies of NZP type of compounds [231]. The anisotropy of axial thermal expansion of these materials is believed to induce micro cracking. A direct correlation between micro cracking of ceramics and their anisotropic axial thermal expansion coefficients was established by employing acoustic emission monitoring techniques [231].

Table 1 Coefficients of thermal expansion for Nasicon type materials in the temperature range RT (room temperature)–500 °C

Composition	Phase	$\alpha \times 10^{-6}$ ($°C^{-1}$)	Reference
$Ca_{0.5}Ti_2(PO_4)_3$	[CTP]	+5.1	[227]
$Ca_{0.5}Zr_2(PO_4)_3$	[CTP]	−1.6	[227]
$Ca_{0.5}ZrTi(PO_4)_3$	[CTP] + ZrP_2O_7	+4.35	[227]
$NaTi_2(PO_4)_3$	[CTP]	−5.5	[227]
$Na_3Cr_2(PO_4)_3$	[CTP]	+5.3	[227]
$NaZr_2(PO_4)_3$	[CTP] + ZrO_2	−4.0	[227]
$Na_{3/2}Zr_{15/8}(PO_4)_3$	[CTP]	−2.35	[227]
$Ca_{0.25}Na_{0.5}Zr_2(PO_4)_3$	[CTP]	+6.3	[227]
$Ca_{0.25}Na_{0.5}Ti_2(PO_4)_3$	[CTP]	+4.0	[227]
$Na_{1.5}Zr_{1.5}Cr_{0.5}(PO_4)_3$	[CTP]	+0.5	[227]
$Mg_{0.5}Zr_2(PO_4)_3$	[NZP]	2.11	[230]
$Ca_{0.5}Zr_2(PO_4)_3$	[NZP]	−2.11	[230]
$Sr_{0.5}Zr_2(PO_4)_3$	[NZP]	3.16	[230]
$Ba_{0.5}Zr_2(PO_4)_3$	[NZP]	3.37	[230]

Thermal expansion studies by high temperature X-ray diffractometry on the composition, $A_{0.5}M_2(PO_4)_3$ (A = Ca or Sr; M = Ti, Zr, Hf, or Sn) were reported by Govindan Kutty et al. DSC measurements on tin compounds indicate the occurrence of a diffuse phase transformation at high temperatures [232]. Woodcock et al. have reported the variable temperature neutron diffraction studies to pinpoint the mechanism of low thermal expansivity in the Nasicon-related material, $Sr_{0.5}Ti_2(PO_4)_3$ [233]. The mechanism of low thermal expansivity in $Sr_{0.5}Ti_2(PO_4)_3$ was established which is in contrast to that observed in $NaZr_2(PO_4)_3$ [231]. Subsequently, they have investigated the variable temperature neutron powder diffraction studies of $K_{0.5}Nb_{0.5}Ti_{1.5}(PO_4)_3$, $Ba_{0.5}Ti_2(PO_4)_3$, and $Ca_{0.25}Sr_{0.25}Zr_2(PO_4)_3$. These compositions exhibit anisotropic low thermal expansion, which is attributed to the thermal expansivity of M1–O bonds [234].

We have reported the preparation, characterization, impedance, and thermal expansion studies of $A_{0.5}MSb(PO_4)_3$ (A = Ca, Mn; M = Al, Fe, and Cr). These materials have been characterized by several methods such as powder XRD, IR, Raman, ESR, ^{31}P-NMR, and Impedance spectroscopy. All these compositions crystallize in Nasicon type lattice. The thermal expansion of these samples is studied in the temperature range 30–500 °C and they exhibit near zero thermal expansion coefficients [235, 236].

Other aspects

It is well known that CO_2 gas is a typical greenhouse effect gas which leads to rise in global temperature. Similarly, sulfur dioxide (SO_2) gas in the global atmosphere is a major source of acid rain. Sulfur dioxide is a toxic gas for human health and destroys the survival environment of human being. In the view of global and environmental safety concerns, the development of CO_2 and SO_2 sensors is very important. Nasicon is a promising material for SO_2 and CO_2 sensors because of its high Na^+ conductivity even at low temperatures, no crack formation upon heating and cooling [237]. The high ionic conductivity of Nasicon is used in the fabrication of sensors where the Nasicon phase acts as solid electrolyte [238]. The electrolyte in combination with an auxiliary phase like metal carbonate or nitrate on one side (to detect CO_2 or NO_2) acts as the sensing electrode and a platinum electrode on the other side acts as reference electrode [239]. Since the original Nasicon composition, $Na_3Zr_2PSi_2O_{12}$ has high ionic conductivity, it is used in the form of dense pellet or thick film in the sensing devices now [240, 241]. Several reports were published based on Nasicon materials as sensors for CO_2, SO_2, NO, NO_2, NH_3, and H_2S gases [237, 242–245]. Proton conducting Nasicon phases like the hydronium Nasicons are used to detect hydrogen in air potentiometrically [246]. Hydronium Nasicons are obtained by the exchange of the mobile Na^+ or Li^+ ions with H^+ ions or with NH_4^+ ions and subsequent heating [50, 247]. Nasicon compositions are also used for immobilization of radioactive waste [248–250], as membranes for ion sensitive electrode and sodium removal from aqueous waste streams [12, 251] and in coupling catalysis [252].

Conclusions

More than one thousand research articles have been published based on Nasicon type materials up to now. Globally, many research groups are still working on this important family for various aspects. Therefore, we have prepared this review with about 252 research articles which cover the most important aspects, i.e., structure, compositional diversity, evolution, synthesis, characterization, and applications of Nasicon type materials at one place.

References

1. Robertson AD, West AR, Ritchie AG (1997) Solid State Ion 104:1
2. Aono H, Imanaka N, Adachi G (1994) Acc Chem Res 27:265 and references there in
3. Weber N, Kummer JT (1967) Proc Annu Power Sources Conf 21:37
4. Whittingham MS, Huggins RA (1971) J Chem Phys 54:414
5. Hong HYP (1976) Mater Res Bull 11:173
6. Goodenough JB, Hong HYP, Kafalas JA (1976) Mater Res Bull 11:203
7. Meunier M, Izquierdo R, Hasnaoui L, Quenneville E, Ivanov D, Girard F, Morin F, Yelon A, Paleologou M (1998) Appl Surf Sci 127–129:466
8. Yao S, Shimizu Y, Miura N, Yamazoe N (1990) Chem Lett 19:2033
9. Gulens J, Longhurst TH, Kuriakose AK, Canaday JD (1988) Solid State Ion 28–30:622
10. Saito Y, Maruyama T (1988) Solid State Ion 28–30:1644
11. Lightfoot P, Woodcock DA, Jorgensen JD, Short S (1999) Int J Inorg Mater 1:53
12. Balagopal S, Landro T, Zecevic S, Sutija D, Elangovan S, Khandkar A (1999) Sep Purif Technol 15:231
13. Brik Y, Kacimi M, Bozon-Verduraz F, Ziyad M (2001) Microporous Mesoporous Mater 43:103
14. Hirose N, Kuwano J (1994) J Mater Chem 4:9
15. Delmas C, Cherkaoui F, Nadiri A, Hagenmuller P (1987) Mater Res Bull 22:631
16. Delmas C, Nadiri A, Soubeyroux JL (1988) Solid State Ion 28–30:419
17. Gopalakrishnan J, Kasturi Rangan K (1992) Chem Mater 4:745
18. Knauth P (2009) Solid State Ion 180:911
19. Ove HL, Peder K (1968) Acta Chem Scand 22:1822
20. Boilot JP, Salanie JP, Desplances G, Le Potier D (1979) Mater Res Bull 14:1469
21. Gordon RS, Miller GR, McEntire BJ, Beck ED, Rasmussen JR (1981) Solid State Ion 3–4:243

22. Schmid H, De Jonghe LC, Cameron C (1982) Solid State Ion 6:57
23. Kuriakose AK, Wheat TA, Ahmed A, DiRocco J (1984) J Am Ceram Soc 67:179
24. von Alpen U, Bell MF, Höffer HH (1981) Solid State Ion 3–4:215
25. Kohler H, Schulz H (1983) Solid State Ion 9–10:795
26. Subramanian MA, Rudolf PR, Clearfield A (1985) J Solid State Chem 60:172
27. Clearfield A, Subramanian MA, Rudolf PR, Moini A (1986) Solid State Ion 18–19:13
28. Alamo J (1993) Solid State Ion 63–65:547
29. Tran Qui D, Capponi JJ, Gondrand M, Saïb M, Joubert JC, Shannon RD (1981) Solid State Ion 3–4:219
30. Bogusz W, Krok F, Piszczatowski W (1999) Solid State Ion 119:145
31. Slade RCT, Young KE, Bonanos N (1991) Solid State Ion 46:83
32. Bogusz W, Frok F, Jakubowsli W (1981) Solid State Ion 2:171
33. Auborn JJ, Johnsonsr DW (1981) Solid State Ion 5:315
34. Kezhionis A, Samulionis V, Skritskij V, Ukshe EA (1989) Solid State Ion 36:235
35. Vaitkus R, Orliukas A, Bukun N, Ukshe E (1989) Solid State Ion 36:231
36. Ivanov-Schitz K, Bykov AB (1997) Solid State Ion 100:153
37. Kreuer D, Kohler H, Warhus U, Schulz H (1986) Mater Res Bull 21:149
38. Clearfield A, Jirustithipong P, Cotman RN, Pack SP (1980) Mater Res Bull 15:1603
39. Clearfield A, Jesus P, Cotman RN (1981) Solid State Ion 5:301
40. Morcrette M, Barboux P, Laurent A, Perriere J (1997) Solid State Ion 93:283
41. Ahmad A, Glasgow C, Wheat TA (1995) Solid State Ion 76:143
42. Izquierodo R, Quenneville E, Trigylidas D, Girand F, Meunier M, Ivanov D, Paleologou M, Yelon A (1997) J Electrochem Soc 144:L323
43. Yoldas BE, Lloyd IK (1983) Mater Res Bull 18:1171
44. Huang YL, Caneiro A, Attari M, Fabry P (1991) Thin Solid Films 196:283
45. Moini A, Clearfield A (1987) Adv Ceram Mater 2:173
46. Perthuis H, Velasco G, Colomban Ph (1984) Jpn J Appl Phys 23:534
47. Shimizu Y, Ushijima T (2000) Solid State Ion 132:143
48. Boilot JP, Colomban Ph (1988) Solid State Ion 28–30:403
49. Gulens J, Hildebrandt BW, Canaday JD, Kuriakose AK, Wheat TA, Ahmad A (1989) Solid State Ion 35:45
50. Canaday JD, Kuriakose AK, Wheat TA, Ahmad A, Gulens J, Hildebrandt BW (1989) Solid State Ion 35:165
51. Ivanov D, Currie J, Bouchard H, Lecours A, Andrian J, Yelon A, Poulin S (1994) Solid State Ion 67:295
52. Boilot JP, Collin G, Comes R (1983) J Solid State Chem 50:91
53. Krimi S, Mansouri I, ElJazouli A, Chaninade JP, Gravereau P, LeFlem G (1993) J Solid State Chem 105:561
54. Visco SJ, Kennedy JH (1983) Solid State Ion 9–10:885
55. Winand JM, Rulmont A, Tarte P (1991) J Solid State Chem 93:341
56. Takahashi T, Kuwabare K, Shibata M (1980) Solid State Ion 1:163
57. Nakamura O, Saito Y, Kodama M, Yamamoto Y (1996) Solid State Ion 89:159
58. Shimazu K, Yamamoto Y, Saito Y, Nakamura O (1995) Solid State Ion 79:106
59. Boguse W, Krok F, Jakubnski W Solid State Ion 9–10:803
60. Krok F, Kony D, Dygas JR, Jakubowski W, Bogusz W (1989) Solid State Ion 36:251
61. Subramanian MA, Rudolf PR, Clearfield A (1885) J Solid State Chem 60:172
62. Feltz A, Barth S (1983) Solid State Ion 9–10:817
63. de la Rochere M, d'Yvoire F, Collin G, Comes R, Boilot JP (1983) Solid State Ion 9–10:825
64. d'Yvoire F, Pintard-Screpel M, Bretey E, de la Rochere M (1983) Solid State Ion 9–10:851
65. Pintard-Screpel M, d'Yvoire F, Remy F (1978) C R Acad Sci Paris 286:381
66. Masquelier C, Wurn C, Rodriguez-Carvazal J, Gaubicher J, Nazar L (2000) Chem Mater 12:525
67. de la Rochere M (1984) Ph. D. Thesis, Universite Pierre et Marie Curie Paris VI, Paris, France
68. Vaidhyanathan B, Rao KJ (1997) J Solid State Chem 132:349
69. Brunet F, Bagdassarov N, Miletich R (2003) Solid State Ion 159:35
70. Aono H, Sugimoto E, Sadaoka Y, Imanaka N, Adachi G (1990) Solid State Ion 40–41:43
71. Shi-Chun L, Zu-Xiang L (1983) Solid State Ion 9–10:835
72. Hamdoune S, Tran Qui D, Schouler EJL (1986) Solid State Ion 18–19:587
73. Govindaraj G, Mariappan CR (2002) Solid State Ion 147:49
74. Losilla R, Aranda MAG, Brequue S, Sanz J, Paris MA, Campo J, West AR (2000) Chem Mater 12:2134
75. Delmas C, Viala JC, Olazcuaga R, Le Flem G, Hagen Muller P (1981) Solid State Ion 3–4:209
76. Brochu R, Cherkaoui F, Delmas C, Olazcuaga R, Le Flem G (1979) C R Acad Sci Paris 289:85
77. Miyajima Y, Miyoshi T, Tamaki J, Matsuoka M, Yamomoto Y, Masquelier C, Tabuchi M, Saito Y, Kageyama H (1999) Sold State Ion 124:201
78. Lu H, Ye J (1997) J Solid State Chem 131:131
79. Barj M, Lucazeau G, Delmas C (1992) J Solid State Chem 100:141
80. Barj M, Perthecis H, Colomban Ph (1983) Solid State Ion 9–10:845
81. Losilla R, Aranda MAG, Breque S, Paris MA, Sanz J, West AR (1998) Chem Mater 10:665
82. Boilot JP, Collin G, Comes R (1983) Solid State Ion 9–10:829
83. Tillement O, Angenault J, Couturier JC, Quarton M (1991) Solid State Ion 44:299
84. Asai T, Ado K, Saito Y, Kageyama H, Nakamura O (1989) Solid State Ion 35:319
85. Saito Y, Ado K, Asai T, Kageyama H, Nakamura O (1992) Solid State Ion 58:327
86. Kageyama H, Kamijo N, Asai T (1990) Solid State Ion 40–41:350
87. Bohnke O, Ronchetti S, Mazza D (1999) Solid State Ion 122:127
88. Wang W, Li D, Zhao J (1992) Solid State Ion 51:97
89. Engell J, Mortensen S, Moller L (1983) Solid State Ion 9–10:877
90. Porkodi P, Yegnaraman V, Kamaraj P, Kalyanavalli V, Jeyakumar D (2008) Chem Mater 20:6410
91. Michele C, Sonia S, Richard I (1999) Solid State Ion 123:173
92. Jauan E, Carlos P (1998) Solid State Ion 112:309
93. Michele C, Sonia S (2000) Solid State Ion 136–137:489
94. Sudreau F, Petit D, Boilot JP (1989) J Solid State Chem 83:78
95. Casciola M, Costantino U, Merlini L, Andersen IGK, Andrersen EK (1988) Solid State Ion 26:229
96. Subramanian MA, Subramaiun R, Clearfield A (1986) Solid State Ion 18–19:562
97. Aono H, Sugimoto E, Sadaoka Y, Imanaka N, Adachi G (1990) Solid State Ion 40–41:38
98. Aono H, Sugimoto E, Sadaoka Y, Imanaka N, Adachi G (1991) Solid State Ion 47:257
99. Zu-xiang L, Hu-jun Y, Shi-chun L, Shun-bao T (1986) Solid State Ion 18–19:549
100. Zu-xiang L, Hu-jun Y, Shi-chun L, Shun-bao T (1988) Solid State Ion 31:91

101. Tran Qui D, Hamdoune S, Soubeyroux JL, Prince E (1988) J Solid State Chem 72:309
102. Tran Qui D, Hamdoune S (1987) Acta Crystallogr C43:397
103. Zaho W, Chen L, Xue R, Min J, Wanqui Cui W (1994) Solid State Ion 70–71:144
104. Martinez-Juarez A, Rojo JM, Iglesias JE, Sanz J (1995) Chem Mater 7:1857
105. Martinez A, Rajo JM, Iglesias JE, Sanz J, Rojas RM (1994) Chem Mater 6:1790
106. Paris MA, Martinez-Juareg A, Iglesias JE, Rojo JM, Sanz J (1997) Chem Mater 9:1430
107. Petit D, Colomban Ph, Collin G, Boilot JP (1986) Mater Res Bull 21:365
108. Kuwano J, Sato N, Kato M, Takano K (1994) Solid State Ion 70–71:332
109. Aono H, Sugimoto E, Sadaoka Y, Imanaka N, Adachi G (1993) Solid State Ion 62:309
110. Losilla ER, Bruque S, Aranda MAG, Moreno-Real L, Morin E, Quarton M (1998) Solid State Ion 112:53
111. Shi-chun L, Jian-yi C, Zu-xiang L (1988) Solid State Ion 28–30:1265
112. Nanjundaswamy KS, Padhi AK, Goodenough JB, Okada S, Ohtsuka H, Arai H, Yamaki J (1996) Solid State Ion 92:1
113. Aono H, Sugimoto E, Sadaoka Y, Imanaka N, Adachi G (1993) J Electrochem Soc 140:1827
114. Ado K, Saito Y, Asai T, Kageyama H, Nakamura O (1992) Solid State Ion 53–56:723
115. Aono H, Sugimoto E, Sadaoka Y, Imanaka N, Adachi GY (1989) J Electrochem Soc 136:590
116. Aono H, Sugimoto E, Sadaoka Y, Imanaka N, Adachi GY (1990) Chem Lett 19:1825
117. Wong S, Newman PJ, Best AS, Nairn KM, MacFarlane DR, Forsyth M (1998) J Mater Chem 8:2199
118. Morin E, Le Mercier T, Quarton M, Losilla ER, Aranda MAG, Breque S (1999) Powder Diffr 14:53
119. Stenina IA, Pinus IY, Rebrov AI, Yaroslavtsev AB (2004) Solid State Ion 175:445
120. Sugantham M, Varadaraju UV (1997) Solid State Ion 95:201
121. Wang S, Hwu SJ (1991) J Solid State Chem 90:377
122. Basu B, Sundaram SK, Maiti HS, Paul A (1986) Solid State Ion 21:231
123. Bykov AB (1990) Solid State Ion 38:31
124. Sigaryov SE, Genkina EA, Maximov BA (1990) Solid State Ion 37:261
125. Sigaryov SE, Terziev VG (1993) Phys Rev B 48:16252
126. Amatucci GG, Safari A, Shokoohi FK, Wilkens BJ (1993) Solid State Ion 60:357
127. Wen Z, Xu X, Li J (2009) J Electroceram 22:342
128. Maud B, Lopez C, Pierre M, Francoise LB, Emmanuelle BS, Jean-Louis F (2008) Dalton Trans 3061
129. Anantharamulu N, Prasad G, Vithal M (2008) Bull Mater Sci 31:133
130. Yao PC, Fray DJ (1983) Solid State Ion 8:35
131. Mbandza A, Bordes E, Courtine P (1985) Mater Res Bull 20:251
132. Bussereau I, Belkhiria MS, Gravereau P, Boireau A, Soubeyroux JL, Olazcuaga R, Le Flem G (1992) Acta Crystallogr C48:1741
133. Oudet F, Vejex A, Company T, Bordes E, Courtine P (1989) Mater Res Bull 24:561
134. Serghini A, Brochu R, Ziyad M, Loukah M, Vedrine JC (1991) J Chem Soc Faraday Trans 87:2487
135. Polles GL, El Jazouli A, Olazcuaga R, Dance JM, Le Flem G, Hagenmuller P (1987) Mater Res Bull 22:1171
136. El Jazouli A, Alami M, Brochu R, Dance JM, Le Flem G, Hagenmuller P (1987) J Solid State Chem 71:444
137. Taoufik I, Haddad M, Brochu R, Berger R (1999) J Mater Sci 34:2943. doi:10.1023/A:1004656023198
138. Taoufik I, Haddad M, Nadiri A, Brochu R, Berger R (1999) J Phys Chem Solids 60:701
139. Fargin E, Bussereau I, Olazcuaga R, Le Flem G, Cartier C, Dexpert H (1994) J Solid State Chem 112:176
140. El Jazouli A, Soubeyroux JL, Dance JM, Le Flem G (1986) J Solid State Chem 65:351
141. Mbandza A, Bordes E, Courtine P, El Jazouli A, Soubeyroux JL, Le Flem G, Hagenmuller P (1988) React Solids 5:315
142. Winand JM, Rulmont A, Tarte P (1993) J Solid State Chem 107:356
143. Serghini A, Brochu R, Olazcuaga R, Gravereau P (1995) Mater Lett 22:149
144. Ziyad M, Ahmamouch R, Rouimi M, Gharbage S, Vedrine JC (1998) Solid State Ion 110:311
145. Vithal M, Srinivasulu B, Koteswara Rao K, Mohan Rao Ch (2000) Mater Lett 45:58
146. Koteswara Rao K, Anantharamulu N, Mishra AK, Bansal C, Vithal M (2005) Solid State Commun 135:692
147. Srinivasulu B, Vithal M (1999) J Mater Sci Lett 18:1771
148. Koteswara Rao K, Bhatnagar AK, Sarkar S, Vithal M (2003) Mater Lett 57:4478
149. Perret R, Boudjada A (1976) Comptes Rendus des Seances de l'Academie des Sciences, Serie C: Sciences Chimiques 282:245
150. Barj M, Perthuis H, Colomban Ph (1983) Solid State Ion 11:157
151. Angenault J, Couturier JC, Quarton M (1989) Mater Res Bull 24:789
152. Masse R (1970) Bull Soc Fr Mineral Cristallogr 93:500
153. Yingjeng JL, Monteith J, Whittingham MS (1991) Solid State Ion 46:337
154. Arsalane S, Ziyad M, Coudurier G, Vedrine JC (1996) J Catal 159:162
155. Koteswara Rao K, Rambabu G, Raghavender M, Prasad G, Kumar GS, Vithal M (2005) Solid State Ion 176:2701
156. Rambabu G, Anantharamulu N, Rao Koteswara K, Prasad G, Vithal M (2008) Mater Res Bull 43:1509
157. Rambabu G, Anantharamulu N, Rao Koteswara K, Sarma JARP, Vithal M (2007) Phys Status Solidi A 204:3454
158. Leclaire A, Borel MM, Grandin A, Raveau B (1991) Mater Res Bull 26:207
159. Leclaire A, Borel MM, Grandin A, Raveau B (1989) Acta Crystallogr C 45:699
160. Delmas C, Olazcuaga R, Cherkaoui F, Brochu R, Le Flem G (1978) C R Acad Sci 287:169
161. Nadiri A, de Doctorat d'Etat T (1986) University of Bordeaux I 18 July
162. Rangan KK, Gopalakrishnan J (1995) Inorg Chem 34:1969
163. Venkataraman T, Ashok KS, Gopalakrishnan J (1999) J Mater Chem 9:739
164. Berry FJ, Vithal M (1995) Polyhedron 14:1113
165. Holland TJB (1980) Am Mineral 65:129
166. Sugantha M, Varadaraju UV, Subba Rao GV (1994) J Solid State Chem 111:33
167. Köhler J, Imanaka N, Adachi G (1998) Chem Mater 10:3790
168. Imanaka N, Adachi G-Y (2002) J Alloys Compd 344:137
169. Tamura S, Egawa T, Okajaki Y, Kobayashi Y, Imanaka N, Adachi G (1998) Chem Mater 10:1958
170. Tamura S, Imanaka N, Adachi G (1999) Adv Mater 11:1521
171. Hasegawa Y, Imanaka N, Adachi G (2003) J Solid State Chem 171:387
172. Imanaka N, Itaya M, Ueda T, Adachi G (2002) Solid State Ion 154–155:319
173. Hasegawa Y, Imanaka N (2006) J Alloy Compd 408–412:661

174. Shinji T, Sudarto, Imanaka N (2009) Kidorui 54:118
175. Nunotani N, Tamura S, Imanaka N (2009) Chem Mater 21:579
176. Tamura S, Itano T, Nunotani N, Imanaka N (2009) Electrochem Solid State Lett 12:F5
177. Nunotani N, Tamura S, Imanaka N (2009) Chem Lett 38:658
178. Nunotani N, Sawada M, Tamura S, Imanaka N (2010) Bull Chem Soc Jpn 83:415
179. Orlova AI, Volgutov VY, Castro GR, Garcia-Granda S, Khainakov SA, Garcia JR (2009) Inorg Chem 48:9046
180. Berry FJ, Costantini N, Smart LE (2006) Solid State Ion 177:2889
181. Chakir M, Jazouli AE, de Wall D (2006) J Solid State Chem 179:1883
182. Chakir M, Jazouli AE, Chaminade JP (2006) Powder Diffr 21:210
183. Salah AA, Jozwiak P, Zaghib K, Garbarczyk J, Gendron F, Mauger A, Julien CM (2006) Spectrochim Acta A 65:1007
184. Marriappan CR, Galven C, Crosnier-Lopez P, Berre FL, Bohnke O (2006) J Solid State Chem 179:450
185. Aatiq A (2004) Powder Diffr 19:272
186. Aatiq A, Dhoum H (2004) Powder Diffr 19:157
187. Fischer W, Singheiser L, Basu D, Dasgupta A (2004) Powder Diff 19:153
188. Aatiq A, Tigha MR, Hassine R, Saadoune I (2006) Powder Diffr 21:45
189. Aatiq A, Hassine R, Tigha MR, Saadoune I (2005) Powder Diffr 20:33
190. Arbi K, Rojo JM, Sanz J (2007) J Eur Ceram Soc 27:4215
191. Essoumhi A, Favotto C, Mansori M, Ouzaouit K, Satre P (2007) Solid State Sci 9:240
192. Benmokhtar S, El Jazouli A, Aatiq A, Chaminade JP, Gravereau P, Wattiaux A, Fournès L, Grenier JC (2007) J Solid State Chem 180:2004
193. Barré M, Crosnier-Lopez MP, Le Berre F, Suard E, Fourquet JL (2007) J Solid State Chem 180:1011
194. Masui T, Koyabu K, Tamura S, Imanaka N (2006) J Alloys Compd 418:73
195. Navulla A (2010) Solid State Ion 181:659
196. Susman S, Delbeeq CJ, McMillan JA (1983) Solid State Ion 9–10:667
197. Sobha KC, Rao KJ (1995) Solid State Ion 81:145
198. Sobha KC, Rao KJ (1996) J Non-Cryst Solids 201:52
199. Sobha KC, Rao KJ (1995) J Chem Sci 107:573
200. Sobha KC, Rao KJ (1996) J Phys Chem Solids 57:1263
201. Prakash GV, Nachimuthu P, Vithal M, Jagannathan R (1999) Bull Mater Sci 22:121
202. Banu T, Koteswara Rao K, Vithal M (2003) Phys Chem Glasses 44:30
203. Prakash GV (2000) Mater Lett 46:15
204. Prakash GV, Jagannathan R, Narayan Rao D (2002) Mater Lett 57:134
205. Govindaraj G, Mariappan CR (2002) Mater Sci Eng B 94:82
206. Mariappan CR, Govidaraj G, Roling B (2005) Solid State Ion 176:723
207. Mariappan CR, Govindaraj G, Vinoth Rathan S, Vijaya Prakash G (2005) Mater Sci Eng B 123:63
208. Xu X, Wen Z, Wu J, Yang X (2007) Solid State Ion 178:29
209. Nagamine K, Hirose K, Honma T, Komatsu T (2008) Solid State Ion 179:508
210. Zhang Q, Wen Z, Liu Y, Song S, Wu X (2009) J Alloys Compd 479:494
211. Okura T, Saimaru M, Monma H, Yamasita K (2009) Solid State Ion 180:537
212. Subba Rao GV, Varadaraju UV, Thomas KA, Sivasankar B (1987) J Solid State Chem 70:101
213. Berry FJ, Tyrer AA, Tyrer EC (1990) Hyperfine Interact 53:297
214. Berry FJ, Greaves C, Marco JF (1992) J Solid State Chem 96:408
215. Berry FJ, Marco JF, Vithal M (1994) Hyperfine Interact 83:351
216. Ohkawa H, Yoshida K, Saito M, Uematsu K, Toda K, Sato M (1999) Chem Lett 1017
217. Barker J, Saidi MY (1999) U. S. Patent 5,871,866
218. Saidi MY, Barker J, Huang H, Swoyer JL, Adamson G (2002) Electrochem Solid State Lett 5:A149
219. Morgan D, Ceder G, Saidi MY, Barker J, Swoyer J, Huang H, Adamson G (2002) Chem Mater 14:4684
220. Morgan D, Ceder G, Saidi MY, Barker J, Swoyer J, Huang H, Adamson G (2003) J Power Sources 119–121:755
221. Yin SC, Grondey H, Strobel P, Huang H, Nazar LF (2003) J Am Chem Soc 125:326
222. Huang H, Yin SC, Kerr T, Taylor N, Nazar LF (2002) Adv Mater 14:1525
223. Aatiq A, Menetrier M, El Jazouli A, Delmas C (2002) Solid State Ion 150:391
224. Aatiq A, Delmas C, El Jazouli A (2001) J Solid State Chem 158:169
225. Alamo J, Roy R (1984) J Am Ceram Soc 67:c78
226. Muller O, Roy R (1974) The major ternary structural families. Springer Verlag, Berlin
227. Roy R, Agrawal DK, Alamo J, Roy RA (1984) Mater Res Bull 19:471
228. Agraval DK, Stubican VS (1985) Mater Res Bull 20:99
229. Lenain GE, Mckinstry HA, Limaye SY, Woodward A (1984) Mater Res Bull 19:1451
230. Limaye SY, Agrawal DK, Mckinstry HA (1987) J Am Ceram Soc 70:c232
231. Srikanth V, Subbarao EC, Agrawal DK, Huang C-Y, Roy R (1991) J Am Ceram Soc 74:365
232. Govindan Kutty KV, Asuvathraman R, Sridharan R (1998) J Mater Sci 33:4007. doi:10.1023/A:1004661132398
233. Woodcock DA, Lightfoot P, Ritter C (1998) Chem Commun 107
234. Woodcock DA, Lightfoot P, Smith RI (1999) J Mater Chem 9:2631
235. Rambabu G, Koteswara Rao K, Anantharamulu N, Raghavender M, Prasad G, Prashanth Kumar V, Vishnuvardhan RC, Vithal M (2007) J Mater Sci 42:3613. doi:10.1007/s10853-006-0400-5
236. Anantharamulua N, Koteswara Rao K, Vithal M, Prasad G (2009) J Alloys Compd 479:619
237. Zhong T, Quan B, Liang X, Liu F, Wang B (2008) Mater Sci Eng B 151:127
238. Maruyama T, Saito Y, Matsumoto Y, Yano Y (1985) Solid State Ion 17:281
239. Pasciak G, Prociow K, Mielcarek W, Gornicka B, Mazurek B (2001) J Eur Ceram Soc 21:1867
240. Qiu F, Zhu Q, Yang X, Quan Y, Sun L (2003) Sens Actuators B 93:237
241. Wang L, Kumar RV (2003) Solid State Ion 158:309
242. Masataka M, Takeo H, Yasuhiro S, Makoto E (2009) Sens Actuators B 139:563
243. Obata K, Matsushima S (2008) Sens Actuators B 130:269
244. Tiegang Z, Xishuang L, Fengmin L, Baofu Q, Geyu L (2008) Chuangan Jishu Xuebao 21:1674
245. Xishuang L, Tiegang Z, Hesong G, Fengmin L, Geyu L, Baofu Q (2009) Sens Actuators B 136:479
246. Maffei N, Kuriakose AK (2004) Sens Actuators B 98:73
247. Clearfield A, Roberts BD, Subramanian MA (1984) Mater Res Bull 19:219
248. Roy R, Vance ER, Alamo J (1982) Mater Res Bull 17:585
249. Scheetz BE, Agrawal DK, Breval E (1994) Wastes Manag (New York) 14:489
250. Nakayama S, Itoh K (2003) J Nucl Sci Technol 40:631
251. Cretin M, Khireddine H, Fabry P (1997) Sens Actuators B 43:224
252. Vernoux P, Gaillard F, Lopez C, Siebert E (2003) J Catal 217:203